PSformer: Parameter-efficient Transformer with Segment Shared Attention for Time Series Forecasting

Anonymous authors
Paper under double-blind review

Abstract

Time series forecasting remains a critical challenge across various domains, often complicated by high-dimensional data and long-term dependencies. This paper presents a novel transformer architecture for time series forecasting, incorporating two innovative designs: parameter sharing module (PS) and Segment Shared Attention (SSA). The proposed model, PSformer, reduces the number of training parameters through the integrated parameter sharing mechanism without sacrificing performance. The spatiotemporal segment defined as a patch spanning across spatial variables and local time. The introduction of SSA could enhance the capability of capturing local spatio-temporal dependencies and improve global representation by integrating information across segments. Consequently, The combination of parameter sharing and SSA reduces the model's parameter count while enhancing forecasting performance. Extensive experiments on benchmark datasets demonstrate that PSformer outperforms many baseline approaches in terms of accuracy and scalability, positioning it as an effective and scalable tool for time series forecasting.

1 Introduction

Time series forecasting is an important learning task with significant application values in a wide range of domains, including the weather prediction Ren et al. (2021); Chen et al. (2023a), traffic flow Tedjopurnomo et al. (2020); Khan et al. (2023), energy consumption Liu et al. (2020); Nti et al. (2020), anomaly detection Zamanzadeh Darban et al. (2022) and the financial analysis Nazareth & Ramana Reddy (2023), etc. With the advancement of artificial intelligence techniques, significant efforts have been devoted to developing innovative models that continue to improve the prediction performance Liang et al. (2024); Wang et al. (2024b). In particular, the transformer-based model family has recently attracted more attention for its proved success in nature language processing OpenAI et al. (2024) and computer vision Liu et al. (2021); Dosovitskiy et al. (2021). Moreover, pre-trained large models based on the transformer architecture have shown advantages in time series forecastingLiu et al. (2024a); Jin et al. (2024); Chang et al. (2023); Woo et al. (2024), demonstrating that increasing the amount of parameters in transformer models and the volume of training data can effectively enhance the model capability.

On the other side, many linear models Zeng et al. (2023); Li et al. (2023) also show competitive performance compared to the complex designs of transformer-based models. One possible reason for their success in time series forecasting is that they have low model complexities and are less likely to overfit on noisy or irrelevant signals. As a result, even with limited data, these models can effectively capture robust information representations. To overcome the limitations of modeling long-term dependencies and capturing complex temporal relationships, PatchTST Nie et al. (2023) process temporal information by combining patching techniques to extract local semantic information, leading to superior performance. However, it applies channel-independent designs and leaves the significant potential for improvement in effectively modeling across variables. Moreover, the unique challenges of modeling multivariate time series data, where the temporal and spatial dimensions differ significantly from other data types, present many unexplored opportunities. While past research donghao & wang xue (2024); Zhang & Yan (2023); Ilbert et al. (2024) has largely treated these dimensions separately, the question of whether systematically mixing temporal and spatial information can further enhance model performance remains an open area for future investigation.

To reduce the model complexity in deep learning, parameter sharing is a crucial technique that can significantly reduce the amount model parameters and enhance computational efficiency. In CNNs, convolutional filters share weights across spatial locations, capturing local features with fewer parameters. Similarly, LSTM networks share weight matrices across time steps to manage memory and control information flow. By studying the sharing of attention weights, Xiao et al. (2019); Kitaev et al. (2020) improved performance in the fields of natural language processing and computer vision. ALBERT Lan et al. (2020) further extends parameter sharing in natural language processing by sharing weights across transformer layers, reducing parameter redundancy while maintaining performance. In multi-task learning, the Task Adaptive Parameter Sharing approach Wallingford et al. (2022) selectively fine-tunes task-specific layers while maximizing parameter sharing across tasks, achieving efficient learning with minimal task-specific modifications. Those studies demonstrate that parameter sharing has the potential for model size reduction, generalization ability enhancement and mitigating the over-fitting risks across various tasks. Besides, employing advanced optimization technique is also essential in reducing the overfitting issue. Ilbert et al. (2024) proposed a simple yet effective transformer-based network and equipped it with the SAM (Sharpness-Aware Minimization) optimization mechanism to achieve competitive performance compared with large models Foret et al. (2021).

In this work, we explore innovative designs of the transformer-based model for time series forecasting by incorporating the spatiotemporal dependencies characteristic of time series tasks and a new parameter sharing model architecture. Some past works have proposed methods to capture spatiotemporal dependency information, such as MOIRAI Woo et al. (2024) flattens multivariate time series by treating all variables as a single sequence, and SAMformer Ilbert et al. (2024), which applies attention to the channel dimension to capture spatial dependencies. Unlike previous methods, we construct a transformer-based model called PSformer, which design as a two-stage SSA structure, each SSA consists of a parameter-sharing design. This parameter-sharing design (as PS Block) consists of three fully connected layers, which keeps the overall number of parameters in both the two-stage SSA and final fusion stage of the PSformer efficient, while also facilitating information sharing between different modules of the model. For SSA, we use patching to divide the variables into different patches, then identify the patches at the same position across different variables and merge them into a segment. As a result, each segment represents the spatial extension of a single-variable patch. In this way, we decompose the multivariate time series into multiple segments. Attention is applied within each segment to enhance the extraction of local spatial-temporal relationships, while information fusion across segments is performed to improve the overall predictive performance. Additionally, by incorporating the SAM optimization method, we further reduce over-fitting while maintaining efficient training. We conduct extensive experiments on long-term time series forecasting datasets to verify the effectiveness of the SSA structure. Our model demonstrates competitive performance in comparison to previous state-of-the-art models, achieving the best performance on 7 out of 8 mainstream long-term time series forecasting tasks. The contributions are summarized as follows:

- We developed a novel transformer-based model structure for time series forecasting, where the parameter sharing technique is applied in the transformer block to reduce the model complexity and improve the generalization ability.
- We proposed a SSA mechanism tailored for multi-variate data, which merges the temporal sequence of different channels to form a local segment and applies attention within each segment to capture both temporal dependencies and cross-channel interactions.
- Through extensive experiments in long-term forecasting tasks and ablation studies, we verified the effectiveness and superior performance of our proposed framework.

2 Related Work

2.1 Temporal modeling in time series forecasting

In recent years, time series analysis has received widespread attention, with more deep learning methods being applied to time series forecasting. These deep learning methods focus on establishing temporal dependencies within time series data to predict future trends. The models can be broadly categorized into RNN-based, CNN-based, MLP-based, and Transformer-based approaches. RNNs and their LSTM variants were widely

used for time series tasks in the past, with related works such as DeepARSalinas et al. (2020). CNN-based methods like TCN Bai et al. (2018) and TimesNet Wu et al. (2023) have been designed to adapt convolutional structures specifically for temporal modeling. MLP-based approaches, such as N-BEATS Oreshkin et al. (2020), RLinear Li et al. (2023), and TSMixer Chen et al. (2023b), have demonstrated that even simple network structures can achieve solid predictive performance. Moreover, Transformer-based models have become increasingly popular in time series forecasting due to the unique attention mechanism of Transformers, which provides strong global modeling capabilities. Many recent works leverage this to enhance time series modeling performance, such as Informer Zhou et al. (2021), Autoformer Wu et al. (2021), Pyraformer Liu et al. (2022), and Fedformer Zhou et al. (2022). Additionally, PatchTST Nie et al. (2023) further divides time series data into different patches to enhance the ability to capture local information. However, the aforementioned models primarily focus on temporal modeling, with less emphasis on modeling the relationships between variables. Although PatchTST attempted to incorporate cross-channel designs, it observed degraded performance in their model.

On the other hand, some pre-trained large models have been applied to time series forecasting tasks Das et al. (2023); Liu et al. (2024a); Gao et al. (2024); Liu et al. (2024c); Zhou et al. (2023); Jin et al. (2024). For example, MOMENT Goswami et al. (2024) uses the patching method and mask pre-training to build a pre-trained model for time series, while GPT4TS Zhou et al. (2023) also adopts the patching method and uses GPT2 as the backbone. The increase in model parameters has provided them with greater expressive power but also increased the difficulty of training.

2.2 Variate modeling in time series forecasting

In addition to modeling temporal dependencies, recent works have focused on modeling inter-variable dependencies donghao & wang xue (2024); Zhang & Yan (2023); Ilbert et al. (2024); Woo et al. (2024); Liu et al. (2024b). ModernTCN donghao & wang xue (2024) employs different 1-D convolutions to capture the temporal and variable dimensions separately; Crossformer Zhang & Yan (2023) constructs attention mechanisms across both time and spatial dimensions; SAMformer Ilbert et al. (2024) applies attention to the variable dimension to model cross-channel dependencies; MORAI Woo et al. (2024) "flattens" multivariate time series into univariate sequences to merge information across variables; iTransformer Liu et al. (2024b) represents multivariate time series and captures global dependencies. All of these works emphasize the simultaneous modeling of both variable and temporal dependencies as critical directions for improving multivariate time series modeling, which helps establish global spatial-temporal dependencies. However, this may weaken the ability to capture local spatial-temporal dependencies. Additionally, expanding the global receptive field of spatio-temporal dependencies could increase model complexity, which in turn may lead to overfitting due to the larger number of parameters. Our work addresses these issues and proposes solutions to mitigate them.

3 The PSformer Framework

3.1 Problem Formulation

As shown in Figure 1, the input multivariate time series is denoted as $X \in \mathbb{R}^{L \times M}$ as with look-back window $L : (x_1, x_2, ..., x_L)$ and M variables, where x_t represents the M-dimensional vector at time step t. L will be equally divided into N non-overlapping patches of size P. $P^{(i)}$ denote the i-th patch with size P, where $i = 1, 2, 3, ..., N$. The $P^{(i)}$ of the M variables forms the i-th segment, which denote cross-channel patch of length C, where $C = M \times P$. The input time series X transformed from $X \in \mathbb{R}^{L \times M}$ to $X \in \mathbb{R}^{C \times N}$ by segment and time series transform (STF). The predict target is the future values of next F time steps, e.g., $(x_{L+1}, ..., x_{L+F})$. Beside, we denote $\boldsymbol{X}^{in}$ and $\boldsymbol{X}^{out}$ as the input and output signals for the specified layers.

3.2 Model Structure

The constructed PSformer model is depicted in Figure 1, where the PSformer Encoder serves as the backbone of the model and the key components of the Encoder include the SSA and PS Block. The PS Block provides the parameters for all layers within the Encoder by utilizing the parameter sharing technique.

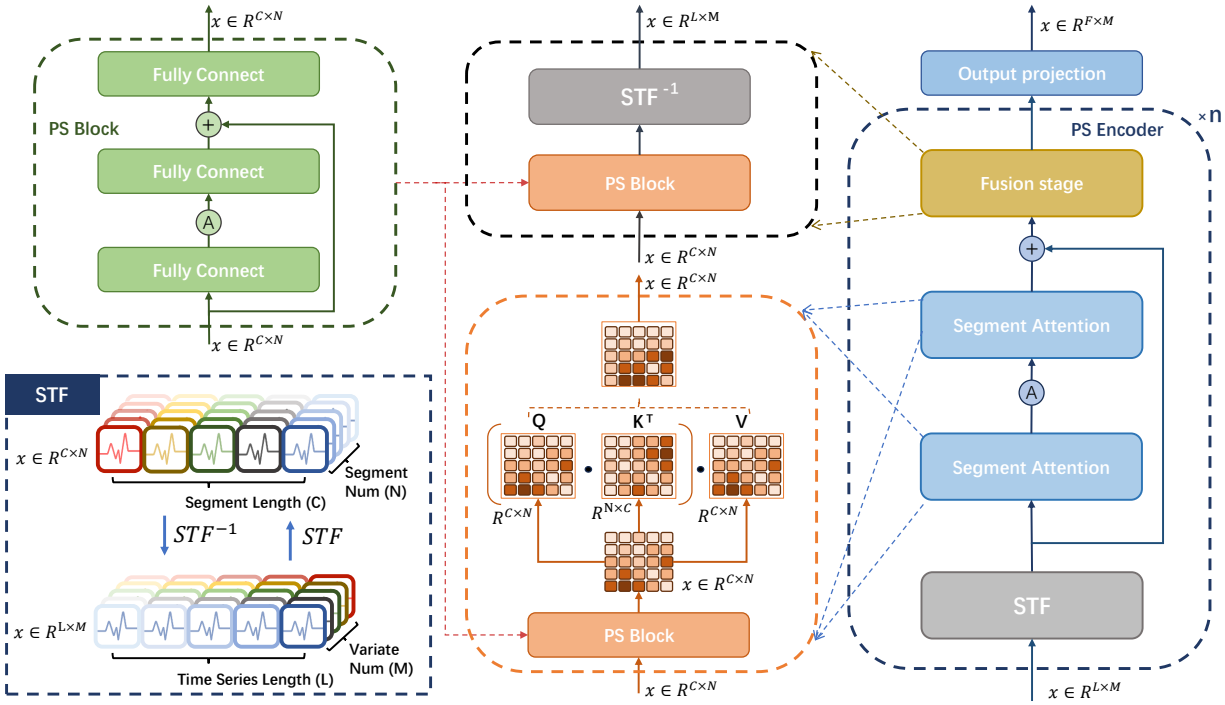

Figure 1: PSformer Network Structure. The PSformer model structure consists of the PS Block, which is composed of three fully connected layers that constitute all network parameters. These parameters are shared across the SSA and fusion stage in the PS Encoder. Through the STF process, SSA constructs an attention matrix along the segment dimension. In the two-stage segment shared attention, the PS Block generates matrices that are simultaneously used as the Q, K, and V matrices for the segment shared attention mechanism. Additionally, in the fusion stage, it further integrates feature information. The parameters of the PS Block form the entirety of the PS Encoder's parameters, which are finally transformed by the output projection for time-series prediction.

Forward Process The univariate time series of length L for the i-th variable, starting at time index 1, is denoted as $x_1^{(i)} = (x_1^{(i)}, ..., x_L^{(i)})$, where $i = 1, ..., M$. Then the input $(x_1, ..., x_L)$ with M dimensions is presented as $x_1 \in \mathbb{R}^{L\times M}$, and x_1 is used as the input to the transformer network structure. Similar to other time series forecasting methods, we use RevIN Kim et al. (2022), which is added at both the input and output of the model.

Segment Shared Attention We introduce segment shared attention (SSA), which aggregates patches from different channels at a local time period into a segment and establishes spatial-temporal relationships across different segments. While the network used to construct the Query, Key, and Value matrices in SSA is implemented by a network with shared parameters and nonlinear activation (PS Block). Specifically, the input time series $X \in \mathbb{R}^{L\times M}$ is first divided into N non-overlapping components along the L dimension, where $L = P \times N$, and transformed into $X \in \mathbb{R}^{(M\times P)\times N}$. By concatenating the M and P dimensions, the input transform to $X \in \mathbb{R}^{C\times N}$, where $C = M \times P$, facilitating the subsequent cross-channel information fusion.

In this transformed space, identical $\boldsymbol{Q} \in \mathbb{R}^{C\times N}$, $\boldsymbol{K} \in \mathbb{R}^{C\times N}$, and $\boldsymbol{V} \in \mathbb{R}^{C\times N}$ matrices are generated by applying a shared block's non-linear projection (applied by PS Block), with weights $\boldsymbol{W} \in \mathbb{R}^{N\times N}$ used to project the input $X^{in} \in \mathbb{R}^{C\times N}$. The $\boldsymbol{Q}$ and $\boldsymbol{K}$ matrices are then multiplied using a dot-product operation to form the attention matrix $\boldsymbol{Q}K^T \in \mathbb{R}^{C\times C}$, which captures relationships between different spatial-temporal segments (in the C dimension) and is used to act on the $\boldsymbol{V}$ matrix. While the computation of $\boldsymbol{Q}$, $\boldsymbol{K}$ and $\boldsymbol{V}$ involves non-linear transformations of the input X^{in} across segments in the N dimension, the scaled

dot-product attention primarily applies attention across the C dimension, allowing the model to focus on dependencies between spatial-temporal segments across channels and time.

This mechanism ensures that information from different segments is integrated through the computation of Q, K, and V. It also captures local spatial-temporal dependencies within individual segments by applying attention to the internal structure of each segment. Additionally, it captures long-term dependencies across segments over larger time steps. The final output is $X^{out} \in \mathbb{R}^{C\times N}$, completing the attention process.

Parameter Shared Block In our work, we propose a novel Parameter Shared Block (PS Block), which consists of three fully connected layers with residual connections, as illustrated in Figure 1. Specifically, we construct three trainable linear mappings $\boldsymbol{W}^{(j)} \in \mathbb{R}^{N\times N}$ with $j \in \{1, 2, 3\}$. The output of the first two layers is computed as:

$$\boldsymbol{X}^{out} = \mathrm{GeLU}(\boldsymbol{X}^{in}\boldsymbol{W}^{(1)})\boldsymbol{W}^{(2)} + \boldsymbol{X}^{in}, \tag{1}$$

which follows a similar structure as the feed-forward network (FFN) with residual connections. This intermediate output $\boldsymbol{X}^{out}$ is then used as the input for the third transformation, yielding

$$\boldsymbol{X}^{out} = \boldsymbol{X}^{in}\boldsymbol{W}^{(3)}. \tag{2}$$

Therefore, the PS Block as a whole can be expressed as:

$$\boldsymbol{X}^{out} = (\mathrm{GeLU}(\boldsymbol{X}^{in}\boldsymbol{W}^{(1)})\boldsymbol{W}^{(2)} + \boldsymbol{X}^{in})\boldsymbol{W}^{(3)}. \tag{3}$$

And we denote PS Block output as $\boldsymbol{X}^{out} = \boldsymbol{X}^{in}\boldsymbol{W}^{S}$, where $W^{S} \in \mathbb{R}^{N\times N}$ and $\boldsymbol{X}^{out} \in \mathbb{R}^{C\times N}$. The structure of the PS Block allows it to perform nonlinear transformations while preserving a linear transformation path. Although the three layers within the PS Block have different parameters, the entire PS Block is reused across different positions in the PSformer Encoder, ensuring that the same block parameters $\boldsymbol{W}^{S}$ are shared across those positions, as illustrated in Figure 1. Specifically, PS Block share parameters across three parts of each PSformer Encoder, which includes two SSA layers and the final PS Block. In the SSA layer, the PS block outputs are used as the Q, K, and V matrices to construct the attention mechanism. This parameter-sharing strategy reduces the overall number of parameters while maintaining the network's expression capacity.

PSformer Encoder In the PSformer Encoder, as shown in Figure 1, each layer shares the same parameters $\boldsymbol{W}^{S}$ of PS Block. For the input $\boldsymbol{X}^{in}$, the transformation in the PSformer Encoder can be expressed as follows:

SSA stage one is represented as: $\boldsymbol{Q}^{(1)} = \boldsymbol{X}^{in}\boldsymbol{W}^{S}$, $\boldsymbol{K}^{(1)} = \boldsymbol{X}^{in}\boldsymbol{W}^{S}$, $\boldsymbol{V}^{(1)} = \boldsymbol{X}^{in}\boldsymbol{W}^{S}$, Therefore, we have $\boldsymbol{Q}^{(1)}$, $\boldsymbol{K}^{(1)}$, $\boldsymbol{V}^{(1)} \in \mathbb{R}^{C\times N}$. The dot-product attention operation can be formulated by

$$\boldsymbol{O}^{(1)} = \mathrm{Softmax}(\frac{\boldsymbol{Q}^{(1)}\boldsymbol{K}^{(1)T}}{\sqrt{d_k}})V^{(1)}, \tag{4}$$

which is followed by the ReLU activation:$\boldsymbol{O}^{(1)}_{act} = ReLU(\boldsymbol{O}^{(1)})$.

SSA stage two is represented as: $\boldsymbol{Q}^{(2)} = \boldsymbol{O}^{(1)}_{act}\boldsymbol{W}^{S}$, $\boldsymbol{K}^{(2)} = \boldsymbol{O}^{(1)}_{act}\boldsymbol{W}^{S}$, $\boldsymbol{V}^{(2)} = \boldsymbol{O}^{(1)}_{act}\boldsymbol{W}^{S}$. Similarly, we have $\boldsymbol{Q}^{(2)}$, $\boldsymbol{K}^{(2)}$, $\boldsymbol{V}^{(2)} \in \mathbb{R}^{C\times N}$, and the dot-product attention operation

$$\boldsymbol{O}^{(2)} = \mathrm{Softmax}(\frac{\boldsymbol{Q}^{(2)}\boldsymbol{K}^{(2)T}}{\sqrt{d_k}})\boldsymbol{V}^{(2)}. \tag{5}$$

The two-stage SSA mechanism can be viewed as analogous to an FFN layer, where the MLP is replaced with attention operations. Additionally, residual connections are introduced between the input and output, and the result is then fed into the final PS Block. Since the transformation in the final PS Block is represented as $\boldsymbol{O}^{out} = \boldsymbol{O}^{in}\boldsymbol{W}^{S}$, the entire encoder can be expressed as

$$\boldsymbol{X}^{out} = (\mathrm{Attention}^{(2)}(\mathrm{ReLU}(\mathrm{Attention}^{(1)}(\boldsymbol{X}^{in}))) + \boldsymbol{X}^{in})\boldsymbol{W}^{S}, \tag{6}$$

with $\boldsymbol{X}^{out} \in \mathbb{R}^{C\times N}$. Finally, since $C = M \times P$ and $L = P \times N$, we apply a dimensionality transformation to obtain $\boldsymbol{X}^{out} \in \mathbb{R}^{L\times M}$.

Table 1: Datasets for long-term forecasting. Dataset size is structured as (Train, Validation, Test).

Dataset	Variate	Predict Length	Frequency	Dataset Size	Information
ETTh1,ETTh2	7	{96,192,336,720}	Hourly	(8545, 2881, 2881)	Electricity
ETTm1,ETTm2	7	{96,192,336,720}	10 mins	(34465, 11521, 11521)	Electricity
Weather	21	{96,192,336,720}	15 mins	(36792, 5271, 10540)	Weather
Electricity	321	{96,192,336,720}	Hourly	(18317, 2633, 5261)	Electricity
Exchange	8	{96,192,336,720}	Daily	(5120, 665, 1422)	Exchange rate
Traffic	862	{96,192,336,720}	Hourly	(12185, 1757, 3509)	Transportation

Table 2: Long-term forecasting task. All the results are averaged from 4 different prediction lengths {96, 192, 336, 720}. A lower MSE or MAE indicates a better performance. See Table B.2 in Appendix for the full results with more baselines.

Metric	PSformer		SAMformer		TSMixer		PatchTST		MOMENT		ModernTCN		FEDformer		GPT4TS		Autoformer		RLinear		iTransformer	
	MSE	MAE	MSE	MAE	MSE	MAE	MSE	MAE	MSE	MAE	MSE	MAE	MSE	MAE	MSE	MAE	MSE	MAE	MSE	MAE	MSE	MAE
ETTh1	0.397	0.418	0.410	0.424	0.420	0.431	0.468	0.455	0.418	0.436	0.421	0.432	0.428	0.454	0.428	0.426	0.473	0.477	0.446	0.434	0.454	0.448
ETTh2	0.338	0.390	0.344	0.391	0.354	0.400	0.387	0.407	0.352	0.394	0.343	0.393	0.388	0.434	0.355	0.395	0.422	0.443	0.374	0.398	0.383	0.407
ETTm1	0.342	0.372	0.373	0.388	0.378	0.392	0.387	0.400	0.344	0.379	0.361	0.384	0.382	0.422	0.351	0.383	0.515	0.493	0.414	0.407	0.407	0.410
ETTm2	0.251	0.313	0.269	0.327	0.283	0.339	0.281	0.326	0.259	0.318	0.262	0.322	0.292	0.343	0.267	0.326	0.310	0.357	0.286	0.327	0.288	0.332
Weather	0.225	0.264	0.261	0.293	0.255	0.289	0.259	0.281	0.228	0.270	0.237	0.274	0.310	0.357	0.237	0.271	0.335	0.379	0.272	0.291	0.258	0.278
Electricity	0.162	0.255	0.181	0.275	0.198	0.296	0.205	0.290	0.165	0.260	0.160	0.255	0.207	0.321	0.167	0.263	0.214	0.327	0.219	0.298	0.178	0.270
Exchange	0.358	0.399	0.445	0.470	0.532	0.523	0.367	0.404	0.437	0.446	0.555	0.536	0.478	0.477	0.371	0.409	0.613	0.539	0.378	0.417	0.360	0.403
Traffic	0.400	0.274	0.425	0.297	0.439	0.315	0.481	0.304	0.415	0.293	0.414	0.283	0.604	0.372	0.414	0.295	0.617	0.384	0.626	0.378	0.428	0.282
Count	7	8	0	0	0	0	1	0	0	0	1	1	0	0	0	0	0	0	0	0	1	1

After passing through n layers of the PSformer Encoder, the final output is $\boldsymbol{X}^{pred} = \boldsymbol{W}^F \boldsymbol{X}^{out}$, where $\boldsymbol{X}^{pred} \in \mathbb{R}^{F \times M}$, $\boldsymbol{W}^F \in \mathbb{R}^{F \times L}$ is a linear mapping and F is the prediction length. The $\boldsymbol{X}^{pred}$ is the final output of the PSformer model. The SSA mixes local spatio-temporal information without the need for positional encoding, and we provide a more detailed discussion in Appendix A.6.

4 Experiment

Datasets In this paper, we focus on the long-term time series forecasting. We follow the time series forecasting work in Ilbert et al. (2024) and use 8 mainstream datasets to evaluate the performance of our proposed PSformer model. As shown in Table 1, these datasets include 4 ETT datasets (ETTh1, ETTh2, ETTm1, ETTm2), as well as Weather, Traffic, Electricity, and Exchange. These datasets have been used as benchmark evaluations in many previous time series forecasting studies.

Baselines We select state-of-the-art (SOTA) models in the field of long-term time series forecasting, including not only Transformer-based models but also large models and other SOTA models. Specifically, baselines include (1) Transformer-based model: SAMformer Ilbert et al. (2024), iTransformer Liu et al. (2024b), PatchTST Nie et al. (2023), FEDformer Zhou et al. (2022), Autoformer Wu et al. (2021), (2) Pretrained Large model: MOMENT Goswami et al. (2024), GPT4TS Zhou et al. (2023), (3) TCN-based model: ModernTCN donghao & wang xue (2024) and (4) MLP-based methods: TSMixer Chen et al. (2023b), RLinear Li et al. (2023). Additionally, we provide more baselines for a comprehensive comparison, including TimeMixer Wang et al. (2024a), CrossGNN Huang et al. (2023), MICN Wang et al. (2023), TimesNet Wu et al. (2023), FITS Xu et al. (2024), Crossformer Zhang & Yan (2023), PDF Dai et al. (2024), and TimeLLM Jin et al. (2024) Further details about these baselines can be found in Appendix B.8.

Experimental Settings The input time series length T is set to 512, and four different prediction lengths $H \in \{96, 192, 336, 720\}$ are used. Evaluation metrics include Mean Squared Error (MSE) and Mean Absolute Error (MAE). We train our constructed models using the SAM optimization technique as in Ilbert et al. (2024). Setting the look-back window of RevIN to 16 for the Exchange dataset, more details about this setting can be found in Appendix B.7. We collect baseline results of SAMformer, TSMixer, FEDformer and Autoformer from Ilbert et al. (2024), in which SAMformer and TSMixer are also trained with SAM, and the results of iTransformer, RLinear and PatchTST from Liu et al. (2024b). We test ModernTCN with the fixed input length of 512 following donghao & wang xue (2024). For the pre-trained large models MOMENT and GPT4TS, the results are collected from Goswami et al. (2024). More details about the baseline settings can be found in Appendix A.2. Besides, We also provide results under uni-variate series and unrelated variate in the Appendix B.6.

4.1 Results and Analysis

Summary of Experimental Results The main experimental results are reported in Table 2. PSformer achieved the best performance on 7 out of 8 major datasets in long-term time series forecasting tasks, demonstrating its strong predictive capabilities across various time series prediction problems. This success is attributed to its SSA mechanism, which enhances the extraction of spatial-temporal information, and the parameter-sharing structure, which improves the model's robustness. The complete experimental results are in Appendix B.2. We also provide additional visualization results to analyze the attention maps across spatial and temporal dimensions in the Appendix B.5.

Comparison with Other SOTA models Compared to other Transformer-based models, PSformer demonstrates higher predictive accuracy, reflecting the effectiveness of dividing multivariate time series data into spatial-temporal segments for attention calculation. The neural network's ability to extract information from all spatial-temporal segments enhances the prediction performance. In contrast to current large pre-trained models, PSformer not only achieves better accuracy but also reduces the amount of parameters through parameter sharing. Although linear models are simpler and have fewer parameters with satisfactory performance in some cases, the ability to extract rich information from complex data is limited. In contrast, PSformer integrates the residual connections, thus enabling a linear path while retaining the capability to process complex nonlinear information. Moreover, the ConvFFN component in ModernTCN tailored for temporal data also confirms that the convolutional mechanism, which actually embodies the idea of parameter sharing, is also effective in the time series domain. With the same spirit, we have successfully applied the parameter sharing to the transformer-based models in the time series field and achieved superior performance.

Comparison with PatchTST and SAMformer PatchTST employs a channel-independent design and divides time series data into multiple patches, which demonstrates the effectiveness of the patching method in time series processing. However, its channel-independent approach does not fully consider the relationships between different channels, focusing only on processing each channel individually. On the other hand, SAMformer applies attention directly to the channel dimension via dimension transformations and utilizes a simplified model structure, achieving good predictive performance. However, it may fail to capture valuable local information without the patching method. PSformer combines the advantages of both models while addressing their limitations. By using SSA, PSformer effectively captures local temporal information and handles relationships among different channels. This design enables PSformer to outperform them in various time series forecasting tasks as validated by extensive experiments.

4.2 Ablation studies

The Effect of segments Numbers Since PSformer employs a non-overlapping patching to construct segments, the model's performance may affected by the number of segments. Therefore, we tested the model's performance with different segment numbers on two datasets, ETTh1, ETTh2 and ETTm1. Given that the input sequence length is fixed at 512, the number of segments must be a divisor of the sequence length. Consequently, we set the number of segments to 8, 16, 32, and 64, and test the model on four different forecasting horizons. The test results are shown in Table 3, which indicate that the number of segments impacts the model's prediction accuracy to some extent, while the differences are relatively small. Across

Table 3: The MSE results of different number of segments (N) on the ETTh1 and ETTm1 dataset.

# of Seg.	ETTh1				ETTm1				ETTh2			
	96	**192**	**336**	**720**	**96**	**192**	**336**	**720**	**96**	**192**	**336**	**720**
8	0.362	0.406	0.670	0.451	0.290	0.325	0.357	0.412	0.273	0.333	0.353	0.387
16	0.352	0.417	0.424	0.446	0.285	0.323	0.353	0.412	0.273	0.333	0.357	0.387
32	0.352	0.386	0.410	0.440	0.282	0.321	0.352	0.413	0.272	0.335	0.356	0.389
64	0.354	0.389	0.412	0.446	0.288	0.325	0.355	0.417	0.275	0.337	0.357	0.394

both datasets, a moderate number of segments (such as 32) tends to perform the balance for both short and long forecasting horizons.

Table 4: The MSE results of different number of encoders on the ETTh1 and ETTm1 dataset.

# of Encoder	ETTh1				ETTm1			
	96	**192**	**336**	**720**	**96**	**192**	**336**	**720**
1	0.352	0.385	0.411	0.440	0.288	0.324	0.356	0.414
2	0.355	0.392	0.418	0.443	0.284	0.323	0.356	0.415
3	0.355	0.391	0.416	0.443	0.282	0.321	0.352	0.413
4	0.355	0.389	0.416	0.440	0.282	0.321	0.353	0.416

The Effect of PSformer Encoder Numbers Since PSformer adopts the SSA mechanism, with non-shared PS Block parameters across different Encoders (shared within Encoder), we tested the impact of varying the number of encoders on model performance. We conducted tests on the ETTh1 and ETTm1 datasets, varying the number of encoders from 1 to 4 with four different forecasting horizons. The experimental results are shown in Table 4. The results indicate that ETTm1 performs best with 3 encoders, while ETTh1 achieves better performance with just 1 encoder. This may suggest that for smaller datasets, fewer encoders result in better performance, as reducing the number of encoders decreases the amount of model parameters, thereby mitigating the risk of over-fitting.

Ablation of Parameter Sharing methods We investigate the impact of parameter-sharing mechanism on the model performance. In addition to the default parameter-sharing approach, which shares parameters only within encoder (`In-Encoder`), we also test the following approaches: a. no parameter sharing, i.e., `None`; b. sharing parameters only across encoders (with different parameters used for the PS blocks within each encoder), i.e., `Cross-Encoders`; and c. sharing parameters both within and across encoders, i.e., `ALL`. We conducted experiments on the ETTm1 and Weather datasets, and the results are shown in Table 5. As can be seen, the `In-Encoder` method performs the best, followed by `ALL`, while `None` shows the worst performance. This indicates that the parameter-sharing mechanism contributes to improving the model performance. Furthermore, we provide a comparison of convergence rates between parameter sharing and non-parameter sharing in Appendix B.9, as well as a comparison of parameter savings achieved by parameter sharing in Appendix B.10 and Appendix A.4.

Ablation of Segment Attention methods As an important component of PSformer, we designed SSA to effectively capture temporal information while fully utilizing the correlations between channels. In the ablation study, we compared different attention mechanisms without using SSA under parameter sharing, as well as the performance of using only MLP. We conducted experiments on the ETTh1 and ETTh2 datasets. In this study, w/o SSA means applying the attention mechanism to the input $x \in \mathbb{R}^{B \times M \times L}$ on the $M \times L$ dimensions. For the setting with channel independence' applies the attention mechanism on the $N \times P$

Table 5: Parameter Sharing with different methods

Sharing Methods		Cross-Encoders	In-Encoder	ALL	None
ETTm1	96	0.297	0.282	0.288	0.295
	196	0.329	0.321	0.326	0.338
	336	0.360	0.352	0.358	0.372
	720	0.420	0.413	0.414	0.425
Weather	96	0.158	0.149	0.151	0.154
	196	0.201	0.193	0.196	0.198
	336	0.252	0.245	0.245	0.245
	720	0.319	0.314	0.316	0.319

Table 6: Ablation analysis of SSA on ETTh1 and ETTh2 (MSE reported). Red: the best.

Variant	ETTh1				ETTh2			
	96	**192**	**336**	**720**	**96**	**192**	**336**	**720**
w SSA (Default)	0.352	0.385	0.411	0.440	0.272	0.335	0.356	0.389
w/o SSA	0.369	0.397	0.414	0.448	0.288	0.365	0.373	0.398
w channel independent	0.376	0.407	0.427	0.455	0.285	0.382	0.369	0.395
only mlp	0.379	0.399	0.426	0.450	0.282	0.352	0.358	0.398

dimensions. The results in Table 6 show the performance of PSformer variants with different attention mechanisms on the ETTh1 and ETTh2 datasets across various forecasting horizons:

- The default PSformer configuration (with SSA) consistently achieves the lowest MSE across all horizons, demonstrating the effectiveness of SSA.
- When SSA is removed, the cross-channel attention is less effective at capturing both local and global temporal dependencies, resulting in slightly increased MSE .
- The variant with channel-independent attention shows further degradation, suggesting that neglecting inter-channel correlations impacts the model's ability to capture temporal features.
- Using only MLP layers also results in higher MSE. Although it performs second best for the three forecasting horizons on ETTh2, it still falls short compared to the performance with SSA, highlighting the necessity of applying SSA.

5 Conclusion and Future Work

In this work, we proposed the PSformer model for multivariate time series forecasting, which leverages SSA to facilitate information transfer among time series variables and capture spatial-temporal dependencies. By employing parameter sharing, the model effectively improves parameter efficiency and reduces the risk of overfitting when the data size is relatively limited. Overall, this designed network structure achieves state-of-the-art performance on long-term multivariate forecasting tasks by enhancing model parameter efficiency and improving the utilization of channel-wise information. Future work can focus on applying these techniques to the development of pre-trained large models for time series forecasting, to overcome the issue of excessively large parameter counts in existing pre-trained models, and improve the capability of extracting information from multivariate time series.

References

Shaojie Bai, J Zico Kolter, and Vladlen Koltun. An empirical evaluation of generic convolutional and recurrent networks for sequence modeling. *arXiv preprint arXiv:1803.01271*, 2018.

Ching Chang, Wen-Chih Peng, and Tien-Fu Chen. LLM4TS: Aligning pre-trained llms as data-efficient time-series forecasters. *arXiv preprint arXiv:2308.08469*, 2023.

Liuyi Chen, Bocheng Han, Xuesong Wang, Jiazhen Zhao, Wenke Yang, and Zhengyi Yang. Machine learning methods in weather and climate applications: A survey. *Applied Sciences*, 13(21), 2023a. ISSN 2076-3417. doi: 10.3390/app132112019.

Si-An Chen, Chun-Liang Li, Sercan O Arik, Nathanael Christian Yoder, and Tomas Pfister. TSMixer: An all-MLP architecture for time series forecast-ing. *Transactions on Machine Learning Research*, 2023b. ISSN 2835-8856.

Tao Dai, Beiliang Wu, Peiyuan Liu, Naiqi Li, Jigang Bao, Yong Jiang, and Shu-Tao Xia. Periodicity decoupling framework for long-term series forecasting. In *The Twelfth International Conference on Learning Representations*, 2024. URL `https://openreview.net/forum?id=dp27P5HBBt`.

Abhimanyu Das, Weihao Kong, Rajat Sen, and Yichen Zhou. A decoder-only foundation model for time-series forecasting. *arXiv preprint arXiv:2310.10688*, 2023.

Luo donghao and wang xue. ModernTCN: A modern pure convolution structure for general time series analysis. In *The Twelfth International Conference on Learning Representations*, 2024. URL `https://openreview.net/forum?id=vpJMJerXHU`.

Alexey Dosovitskiy, Lucas Beyer, Alexander Kolesnikov, Dirk Weissenborn, Xiaohua Zhai, Thomas Unterthiner, Mostafa Dehghani, Matthias Minderer, Georg Heigold, Sylvain Gelly, Jakob Uszkoreit, and Neil Houlsby. An image is worth 16x16 words: Transformers for image recognition at scale. In *International Conference on Learning Representations*, 2021.

Pierre Foret, Ariel Kleiner, Hossein Mobahi, and Behnam Neyshabur. Sharpness-aware minimization for efficiently improving generalization. In *International Conference on Learning Representations*, 2021.

Shanghua Gao, Teddy Koker, Owen Queen, Thomas Hartvigsen, Theodoros Tsiligkaridis, and Marinka Zitnik. UniTS: Building a unified time series model. *arXiv preprint arXiv:2403.00131*, 2024.

Mononito Goswami, Konrad Szafer, Arjun Choudhry, Yifu Cai, Shuo Li, and Artur Dubrawski. MOMENT: A family of open time-series foundation models. In *Forty-first International Conference on Machine Learning*, 2024. URL `https://openreview.net/forum?id=FVvf69a5rx`.

Qihe Huang, Lei Shen, Ruixin Zhang, Shouhong Ding, Binwu Wang, Zhengyang Zhou, and Yang Wang. CrossGNN: Confronting noisy multivariate time series via cross interaction refinement. In *Thirty-seventh Conference on Neural Information Processing Systems*, 2023.

Romain Ilbert, Ambroise Odonnat, Vasilii Feofanov, Aladin Virmaux, Giuseppe Paolo, Themis Palpanas, and Ievgen Redko. SAMformer: Unlocking the potential of transformers in time series forecasting with sharpness-aware minimization and channel-wise attention. In *Forty-first International Conference on Machine Learning*, 2024. URL `https://openreview.net/forum?id=8kLzL5QBh2`.

Ming Jin, Shiyu Wang, Lintao Ma, Zhixuan Chu, James Y. Zhang, Xiaoming Shi, Pin-Yu Chen, Yuxuan Liang, Yuan-Fang Li, Shirui Pan, and Qingsong Wen. Time-LLM: Time series forecasting by reprogramming large language models. In *The Twelfth International Conference on Learning Representations*, 2024. URL `https://openreview.net/forum?id=Unb5CVPtae`.

Anwar Khan, Mostafa M Fouda, Dinh-Thuan Do, Abdulaziz Almaleh, and Atiq Ur Rahman. Short-term traffic prediction using deep learning long short-term memory: Taxonomy, applications, challenges, and future trends. *IEEE Access*, 11:94371–94391, 2023.

Taesung Kim, Jinhee Kim, Yunwon Tae, Cheonbok Park, Jang-Ho Choi, and Jaegul Choo. Reversible instance normalization for accurate time-series forecasting against distribution shift. In *International Conference on Learning Representations*, 2022. URL https://openreview.net/forum?id=cGDAkQo1C0p.

Nikita Kitaev, Lukasz Kaiser, and Anselm Levskaya. Reformer: The efficient transformer. In *International Conference on Learning Representations*, 2020. URL https://openreview.net/forum?id=rkgNKkHtvB.

Zhenzhong Lan, Mingda Chen, Sebastian Goodman, Kevin Gimpel, Piyush Sharma, and Radu Soricut. Albert: A lite bert for self-supervised learning of language representations. In *International Conference on Learning Representations*, 2020. URL https://openreview.net/forum?id=H1eA7AEtvS.

Zhe Li, Shiyi Qi, Yiduo Li, and Zenglin Xu. Revisiting long-term time series forecasting: An investigation on linear mapping, 2023. URL https://arxiv.org/abs/2305.10721.

Yuxuan Liang, Haomin Wen, Yuqi Nie, Yushan Jiang, Ming Jin, Dongjin Song, Shirui Pan, and Qingsong Wen. Foundation models for time series analysis: A tutorial and survey. In *Proceedings of the 30th ACM SIGKDD Conference on Knowledge Discovery and Data Mining*, pp. 6555–6565, 2024.

Che Liu, Bo Sun, Chenghui Zhang, and Fan Li. A hybrid prediction model for residential electricity consumption using holt-winters and extreme learning machine. *Applied Energy*, 275:115383, 2020. ISSN 0306-2619.

Shizhan Liu, Hang Yu, Cong Liao, Jianguo Li, Weiyao Lin, Alex X. Liu, and Schahram Dustdar. Pyraformer: Low-complexity pyramidal attention for long-range time series modeling and forecasting. In *International Conference on Learning Representations*, 2022. URL https://openreview.net/forum?id=0EXmFzUn5I.

Xu Liu, Junfeng Hu, Yuan Li, Shizhe Diao, Yuxuan Liang, Bryan Hooi, and Roger Zimmermann. UniTime: A language-empowered unified model for cross-domain time series forecasting. In *Proceedings of the ACM on Web Conference 2024*, pp. 4095–4106, 2024a.

Yong Liu, Tengge Hu, Haoran Zhang, Haixu Wu, Shiyu Wang, Lintao Ma, and Mingsheng Long. iTransformer: Inverted transformers are effective for time series forecasting. In *The Twelfth International Conference on Learning Representations*, 2024b. URL https://openreview.net/forum?id=JePfAI8fah.

Yong Liu, Haoran Zhang, Chenyu Li, Xiangdong Huang, Jianmin Wang, and Mingsheng Long. Timer: Transformers for time series analysis at scale. *arXiv preprint arXiv:2402.02368*, 2024c.

Ze Liu, Yutong Lin, Yue Cao, Han Hu, Yixuan Wei, Zheng Zhang, Stephen Lin, and Baining Guo. Swin transformer: Hierarchical vision transformer using shifted windows. In *Proceedings of the IEEE/CVF International Conference on Computer Vision (ICCV)*, pp. 10012–10022, October 2021.

Noella Nazareth and Yeruva Venkata Ramana Reddy. Financial applications of machine learning: A literature review. *Expert Systems with Applications*, 219:119640, 2023. ISSN 0957-4174.

Yuqi Nie, Nam H. Nguyen, Phanwadee Sinthong, and Jayant Kalagnanam. A time series is worth 64 words: Long-term forecasting with transformers. In *International Conference on Learning Representations*, 2023.

Isaac Kofi Nti, Moses Teimeh, Owusu Nyarko-Boateng, and Adebayo Felix Adekoya. Electricity load forecasting: a systematic review. *Journal of Electrical Systems and Information Technology*, 7:1–19, 2020.

OpenAI, Josh Achiam, Steven Adler, Sandhini Agarwal, Lama Ahmad, Ilge Akkaya, Florencia Leoni Aleman, and Diogo Almeida. Gpt-4 technical report, 2024.

Boris N. Oreshkin, Dmitri Carpov, Nicolas Chapados, and Yoshua Bengio. N-beats: Neural basis expansion analysis for interpretable time series forecasting. In *International Conference on Learning Representations*, 2020. URL https://openreview.net/forum?id=r1ecqn4YwB.

Xiaoli Ren, Xiaoyong Li, Kaijun Ren, Junqiang Song, Zichen Xu, Kefeng Deng, and Xiang Wang. Deep learning-based weather prediction: A survey. *Big Data Research*, 23:100178, 2021. ISSN 2214-5796. doi: https://doi.org/10.1016/j.bdr.2020.100178.

David Salinas, Valentin Flunkert, Jan Gasthaus, and Tim Januschowski. Deepar: Probabilistic forecasting with autoregressive recurrent networks. *International journal of forecasting*, 36(3):1181–1191, 2020.

David Alexander Tedjopurnomo, Zhifeng Bao, Baihua Zheng, Farhana Murtaza Choudhury, and Alex Kai Qin. A survey on modern deep neural network for traffic prediction: Trends, methods and challenges. *IEEE Transactions on Knowledge and Data Engineering*, 34(4):1544–1561, 2020.

Matthew Wallingford, Hao Li, Alessandro Achille, Avinash Ravichandran, Charless Fowlkes, Rahul Bhotika, and Stefano Soatto. Task adaptive parameter sharing for multi-task learning. In *2022 IEEE/CVF Conference on Computer Vision and Pattern Recognition (CVPR)*, pp. 7551–7560, 2022. doi: 10.1109/CVPR52688.2022.00741.

Huiqiang Wang, Jian Peng, Feihu Huang, Jince Wang, Junhui Chen, and Yifei Xiao. MICN: Multi-scale local and global context modeling for long-term series forecasting. In *The Eleventh International Conference on Learning Representations*, 2023.

Shiyu Wang, Haixu Wu, Xiaoming Shi, Tengge Hu, Huakun Luo, Lintao Ma, James Y. Zhang, and JUN ZHOU. Timemixer: Decomposable multiscale mixing for time series forecasting. In *The Twelfth International Conference on Learning Representations*, 2024a.

Yuxuan Wang, Haixu Wu, Jiaxiang Dong, Yong Liu, Mingsheng Long, and Jianmin Wang. Deep time series models: A comprehensive survey and benchmark. *arXiv preprint arXiv:2407.13278*, 2024b.

Gerald Woo, Chenghao Liu, Akshat Kumar, Caiming Xiong, Silvio Savarese, and Doyen Sahoo. Unified training of universal time series forecasting transformers. *arXiv preprint arXiv:2402.02592*, 2024.

Haixu Wu, Jiehui Xu, Jianmin Wang, and Mingsheng Long. Autoformer: Decomposition transformers with Auto-Correlation for long-term series forecasting. In *Advances in Neural Information Processing Systems*, 2021.

Haixu Wu, Tengge Hu, Yong Liu, Hang Zhou, Jianmin Wang, and Mingsheng Long. Timesnet: Temporal 2d-variation modeling for general time series analysis. In *The Eleventh International Conference on Learning Representations*, 2023. URL `https://openreview.net/forum?id=ju_Uqw384Oq`.

Tong Xiao, Yinqiao Li, Jingbo Zhu, Zhengtao Yu, and Tongran Liu. Sharing attention weights for fast transformer. pp. 5292–5298. International Joint Conferences on Artificial Intelligence Organization, 7 2019. doi: 10.24963/ijcai.2019/735.

Zhijian Xu, Ailing Zeng, and Qiang Xu. FITS: Modeling time series with $10k$ parameters. In *The Twelfth International Conference on Learning Representations*, 2024. URL `https://openreview.net/forum?id=bWcnvZ3qMb`.

Zahra Zamanzadeh Darban, Geoffrey I Webb, Shirui Pan, Charu Aggarwal, and Mahsa Salehi. Deep learning for time series anomaly detection: A survey. *ACM Computing Surveys*, 2022.

Ailing Zeng, Muxi Chen, Lei Zhang, and Qiang Xu. Are transformers effective for time series forecasting? AAAI Press, 2023. ISBN 978-1-57735-880-0. doi: 10.1609/aaai.v37i9.26317.

Yunhao Zhang and Junchi Yan. Crossformer: Transformer utilizing cross-dimension dependency for multivariate time series forecasting. In *The Eleventh International Conference on Learning Representations*, 2023. URL `https://openreview.net/forum?id=vSVLM2j9eie`.

Haoyi Zhou, Shanghang Zhang, Jieqi Peng, Shuai Zhang, Jianxin Li, Hui Xiong, and Wancai Zhang. Informer: Beyond efficient transformer for long sequence time-series forecasting. In *Proceedings of the AAAI conference on artificial intelligence*, number 12, pp. 11106–11115, 2021.

Tian Zhou, Ziqing Ma, Qingsong Wen, Xue Wang, Liang Sun, and Rong Jin. Fedformer: Frequency enhanced decomposed transformer for long-term series forecasting. In *International conference on machine learning*, pp. 27268–27286. PMLR, 2022.

Tian Zhou, Peisong Niu, Xue Wang, Liang Sun, and Rong Jin. One fits all: Power general time series analysis by pretrained LM. In *Thirty-seventh Conference on Neural Information Processing Systems*, 2023.

A Experimental Configuration

A.1 Hardware

All experiments were conducted on two servers, each equipped with an 80GB NVIDIA A100 GPU and 4 Intel Xeon Gold 5218 CPUs.

A.2 Details of Baseline Settings

We conducted all of our experiments with look-back window $L = 512$ and prediction horizons $H \in \{96, 192, 336, 720\}$. Results of PSformer and ModernTCN reported in Table 12 come from our own experiments. The difference between our experiment with ModernTCN and its official code is that we standardized the look-back window to 512 and set *drop_last=False* for the test set in the dataloader to ensure consistency with our experimental settings for a fair comparison. For MOMENT and GPT4TS, the results are collected from Goswami et al. (2024), except Exchange rate (which is tested on official code repository). The results of SAMformer, TSMixer, FEDformer and Autoformer are obtained from Ilbert et al. (2024), while the results of iTransformer, PatchTST, and RLinear are taken from Liu et al. (2024b).

A.3 Settings for PSformer

We provides an overview of the experimental configurations for the PSFormer model across various tasks and datasets in Table 7. The experiments cover multiple time-series datasets, including ETTh1, ETTh2, ETTm1, ETTm2, Weather, Electricity, Traffic, and Exchange. In all experiments, the input sequence length (Input Length T) is set to 512, and each input is equally divided into 32 non-overlapping segments (Segments Num. N). The model architecture uses 3 Encoders for tasks, while for the ETTh1, ETTh2, ETTm2 and Exchange, 1 Encoder are used.

The learning rate adjustment strategy (schedule) is set to “constant" for all experiments, with a fixed learning rate (LR) of 10^{-4}. The loss function used in all experiments is Mean Squared Error (MSE). The batch size is set to 16 for most tasks, except for the Traffic dataset, where the batch size is 8. Each experiment runs for 300 epochs, with a patience value of 30 for early stopping. A fixed random seed of 1 is applied across all experiments to ensure reproducibility.

Table 7: An overview of the experimental configurations for PSformer.

Task-Dataset	Encoder Num.	Input Length T	Segment Num. N	schedule	LR*	Loss	Batch Size	Epochs	patient	random seed
ETTh1	1	512	32	constant	10^{-4}	MSE	16	300	30	1
ETTh2	1	512	32	constant	10^{-4}	MSE	16	300	30	1
ETTm1	3	512	32	constant	10^{-4}	MSE	16	300	30	1
ETTm2	1	512	32	constant	10^{-4}	MSE	16	300	30	1
Weather	3	512	32	constant	10^{-4}	MSE	16	300	30	1
Electricity	3	512	32	constant	10^{-4}	MSE	16	300	30	1
Traffic	3	512	32	constant	10^{-4}	MSE	8	300	30	1
Exchange	1	512	32	constant	10^{-4}	MSE	16	300	30	1

A.4 Model Size Comparison

Table 8 presents a comparison of the parameter size across different models, including the PSFormer and other baseline models such as SAMformer, TSMixer, ModernTCN, and RLinear. The comparison is conducted on ETTh1, Weather, and Traffic datasets, with prediction horizons $H \in \{96, 192, 336, 720\}$. PSFormer is evaluated in two configurations: the full model and the encoder part. The parameters of the encoder part refer to the number of parameters after excluding the linear mapping in the output layer. The table denote that both PSFormer (full) and SAMformer have parameter sizes that are close to RLinear, where RLinear's parameters mainly stem from the linear mapping between input and output. Notably, the parameter sizes of these three models are relatively unaffected by the number of input channels. In contrast, TSMixer and ModernTCN exhibit significantly larger parameter sizes, with the number of input channels playing a major

Table 8: Comparison of the trainable model parameters

Dataset	Horizon	PSformer		SAMformer	TSMixer	ModernTCN	RLinear
		Full	*Encoder*				
ETTh1	H=96	52,416	3,168	50,272	124,142	876,064	49248
	H=192	101,664	3,168	99,520	173,390	1,662,592	98496
	H=336	175,536	3,168	173,392	247,262	2,842,384	172368
	H=720	372,528	3,168	369,904	444,254	5,988,496	369360
Relative Size (Avg)		1.0	0.014	0.987	1.408	16.192	0.948
Weather	H=96	58,752	9,504	50,272	121,908	2,709,280	49248
	H=192	108,000	9,504	99,520	171,156	3,495,808	98496
	H=336	181,872	9,504	173,392	245,028	4,675,600	172368
	H=720	378,864	9,504	369,904	442,020	7,821,712	369360
Relative Size (Avg)		1.0	0.039	0.953	1.347	25.708	0.948
Traffic	H=96	58,752	9,504	50,272	793,424	822,018,208	49248
	H=192	108,000	9,504	99,520	842,672	822,804,736	98496
	H=336	181,872	9,504	173,392	916,544	823,984,528	172368
	H=720	378,864	9,504	369,904	1,113,536	827,130,640	369360
Relative Size (Avg)		1.0	0.039	0.953	5.040	4530.574	0.948

role in the overall parameter burden. The relative size comparison shows that TSMixer and ModernTCN have several times, or even thousands of times, more parameters than PSFormer(full). Finally, the parameter size of PSFormer(Encoder) is much smaller, indicating that optimizing the linear mapping layer in the output could further reduce the overall parameter count.

A.5 Running time Comparison

The average running time per iteration (s/iter) of different models on the ETTh1 and Weather datasets with varying prediction horizons is shown in Table 9. PSformer demonstrates relatively stable running times across different horizons. For the ETTh1 dataset, the running time remains between 0.011 and 0.012 seconds, while for the Weather dataset, it varies slightly between 0.026 and 0.027 seconds. PSformer also shows comparatively efficient running times across the datasets, with performance that remains competitive even as the prediction horizon increases. This indicates that PSformer manages computational costs effectively, especially when compared to more complex models.

Table 9: Comparison of the running time (s/iter). We test the average running time per iteration of different models across the first five epochs on the ETTh1 and Weather datasets.

Dataset	Horizon	PSformer	PatchTST	ModernTCN	TSMixer	RLinear	iTransformer
ETTh1	H=96	0.012	0.049	0.241	0.013	0.032	0.020
	H=192	0.011	0.049	0.244	0.016	0.033	0.023
	H=336	0.012	0.054	0.245	0.015	0.034	0.022
	H=720	0.012	0.063	0.279	0.019	0.037	0.025
Weather	H=96	0.026	0.165	0.388	0.013	0.030	0.022
	H=192	0.026	0.166	0.361	0.016	0.032	0.022
	H=336	0.027	0.176	0.730	0.016	0.033	0.027
	H=720	0.027	0.185	0.788	0.024	0.034	0.035

Table 10: Performance comparison with different positional embedding methods.

Dataset	Horizon	Pos emb (time series)	Pos emb (segment)	No pos emb
ETTh1	96	0.378	0.353	0.352
	192	0.412	0.388	0.385
ETTh2	96	0.298	0.276	0.272
	192	0.352	0.338	0.335
Exchange Rate	96	0.189	0.095	0.091
	192	0.314	0.201	0.197
	336	0.525	0.370	0.345
	720	1.574	1.041	1.036

A.6 Discuss about Positional Encoding

The reasons of eliminating positional encoding On the one hand, the SAMformer does not use positional encoding because it applies attention to the channel dimension, where there is no strict sequential relationship between channels. Although SSA in PSformer is also a cross-channel structure, it involves local time series constructed by patches. We consider such local sequences as local representations (or tokens) rather than short sequences. The experimental results also demonstrate that this structure can similarly reduce the dependency on positional encoding while achieving good performance.

On the other hand, we conducted a set of comparative experiments using positional encoding to better illustrate its impact. Specifically, we tested the encoding performance under two different data transformation modes: pos emb (time series), where positional encoding is applied to the original time series before dimension transformation; and pos emb (segment), where positional encoding is applied to the transformed segments. The default case, No pos emb, refers to the absence of positional encoding.

To highlight the differences between seasonal vs. non-seasonal and stationary vs. non-stationary characteristics, we selected the ETTh1 and ETTh2 datasets (relatively seasonal and stable) as well as the Exchange dataset (relatively non-seasonal and non-stationary). The experimental results are shown in the Table 10.

The degraded performance of pos emb (time series) might be due to the incompatibility of the positional encoding with dimension transformation, as the original temporal order is lost in the segment dimension, making it unsuitable for dot-product attention calculations. On the other hand, pos emb (segment) shows smaller changes compared to the No pos emb case, but the performance still deteriorates slightly. This suggests that the significance of positional encoding in the context of multivariate time series forecasting might need to be re-evaluated, as there are fundamental differences between NLP and time series data when applying attention mechanisms.

A.7 Sharpness-Aware Minimization (SAM)

Optimization steps SAM optimizer Foret et al. (2021) modifies the typical gradient descent update to seek a flatten optimum. Below is the mathematical formulation:

Let θ be the model parameters, $\mathcal{L}(\theta)$ be the loss function, and ϵ be a small perturbation applied to the parameters. The SAM optimization process can be described in two steps:

- Find the adversarial perturbation that maximizes the loss in a neighborhood of the current weights θ:

$$\hat{\epsilon} = \arg\max_{\|\epsilon\| \leq \rho} \mathcal{L}(\theta + \epsilon)$$

  where ρ is a small constant that controls the size of the neighborhood.

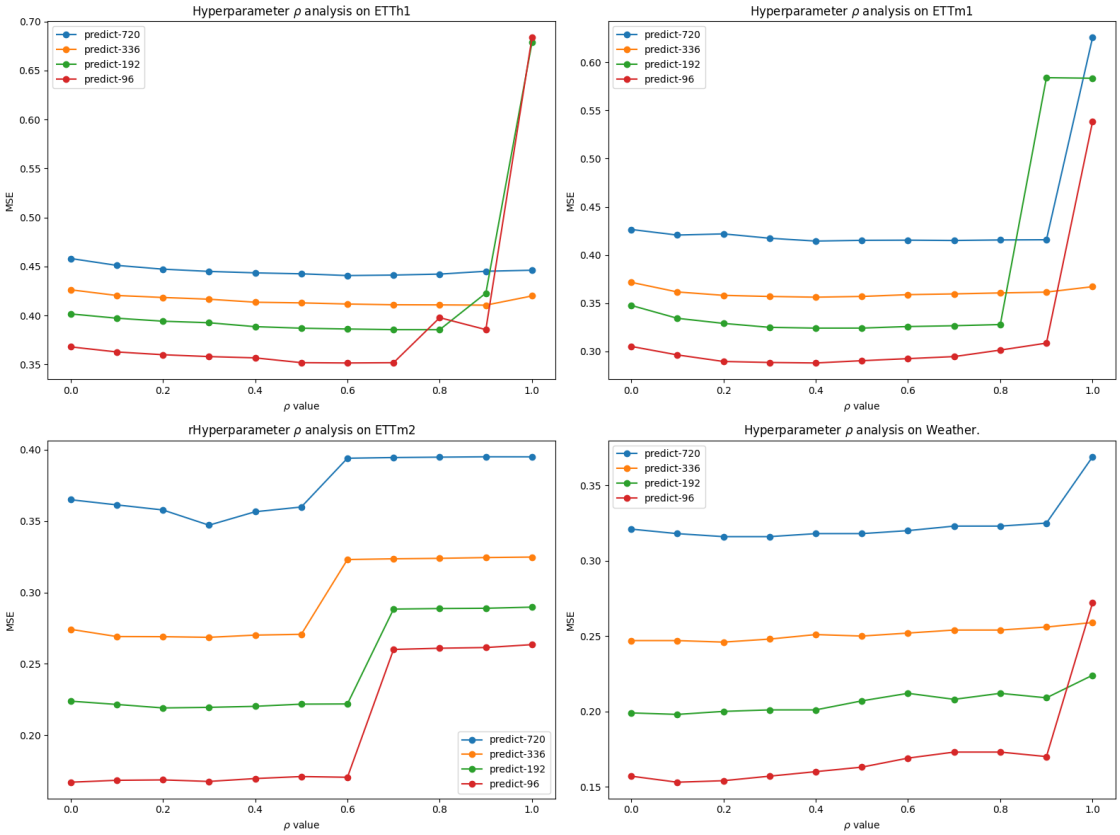

Figure 2: Ablation analysis on hyper-parameter ρ. When taking ρ values from 0 to 1 in steps of 0.1, the prediction loss will slightly decrease first and then increase significantly if the ρ exceeds a threshold, which means the selection of ρ should be careful.

- Update the parameters in the direction that minimizes the loss with respect to the perturbed parameters:

$$\theta \leftarrow \theta - \eta \nabla_\theta \mathcal{L}(\theta + \hat{\epsilon})$$

  where η is the learning rate.

As used in SAMformer, we also employ this optimization technique to train our models, which can generate promising results.

B More Results and Analysis

B.1 Investigation of hyper-parameter ρ

The Effect of ρ. Since we employed SAM to ensure training stability, we also conducted sensitivity tests on the hyper-parameter ρ in SAM. We divided the range of ρ from 0 to 1 into 10 equal parts and tested its effect on model prediction performance across the ETTh1, ETTm1, ETTm2, and Weather datasets. The results are shown in Figure 2. It can be observed that as the parameter ρ gradually increases in SAM can improve the model's prediction performance to some extent. However, if ρ is set too large, it may degrade the model's performance. When selecting ρ, it's important to consider the dataset's complexity and noise levels, as well as the model's architecture. For more complex datasets or larger models, a slightly larger ρ can help smooth the loss landscape and improve generalization. Further, ρ should also be balanced with the learning rate to avoid instability or performance degradation. As a comparison, we also report the ρ^* used by *PSformer*, *SAMformer* and *TSMixer* in the Table 11.

Table 11: Neighborhood size ρ^* used by *PSformer*, *SAMformer* and *TSMixer* for SAM optimization to achieve their best performance on the benchmarks.

H	Model	ETTh1	ETTh2	ETTm1	ETTm2	Electricity	Exchange	Traffic	Weather
96	*PSformer*	0.6	0.1	0.4	0.0	0.0	0.2	0.1	0.1
	SAMformer	0.5	0.5	0.6	0.2	0.5	0.7	0.8	0.4
	TSMixer	1.0	0.9	1.0	1.0	1.0	0.9	0.0	0.5
192	*PSformer*	0.8	0.0	0.4	0.2	0.1	0.1	0.1	0.1
	SAMformer	0.6	0.8	0.9	0.9	0.6	0.8	0.1	0.4
	TSMixer	0.7	0.1	0.6	0.9	0.6	0.9	0.9	0.4
336	*PSformer*	0.9	0.6	0.4	0.3	0.1	0.2	0.2	0.2
	SAMformer	0.9	0.6	0.9	0.8	0.5	0.5	0.5	0.6
	TSMixer	0.7	0.7	0.9	1.0	0.4	1.0	0.6	0.6
720	*PSformer*	0.6	0.5	0.4	0.3	0.1	0.2	0.3	0.3
	SAMformer	0.9	0.8	0.9	0.9	1.0	0.9	0.7	0.5
	TSMixer	0.3	0.4	0.5	1.0	0.9	0.1	0.9	0.3

B.2 Full Results

Table 12 presents the detailed experimental results of different models and forecasting horizons, providing a comprehensive evaluation of their performance in long-term time series forecasting tasks. The performance is measured using Mean Squared Error (MSE) and Mean Absolute Error (MAE). In the table, red values represent the best performance in the respective task and metric, while blue-lined values indicate the second-best performance.

The last row of the table summarizes the number of first-place results for each model across all tasks. As can be seen, PSformer achieved the best MSE performance in 20 out of 32 prediction tasks, and ranked second in 8 tasks. In terms of MAE, PSformer achieved the best results in 22 tasks and came second in 5 tasks. This clearly demonstrates the superior performance of PSformer compared to other baseline models in long-term time series forecasting tasks.

The next best-performing model is ModernTCN, which achieved the best MSE results in 6 tasks and the best MAE results in 3 tasks. While other models such as SAMformer and PatchTST also showed competitive performance in some tasks, their overall results are not as strong as those of PSformer and ModernTCN. In summary, PSformer's strong performance across multiple benchmark tasks suggests its potential effectiveness in long-term forecasting.

B.3 Training loss

Figure 3 illustrates the training and validation loss curves of the ETTh1 and ETTm1 datasets with prediction horizons $H = \{96, 192\}$. In this experiment, we set the number of epochs to 200 and disabled early stopping to observe the complete training process. As shown in the plots, despite the model reaching convergence early in the training (as indicated by the flattening of the training loss curve), the validation loss remains consistently low throughout the training duration. This indicates the model's stability and its ability to generalize well to unseen data over extended epochs.

B.4 Visualization

To better understand our method, we present the forecast curves and the corresponding attention maps for several selected samples. The attention maps visualize the attention weights in different stages of the model, providing insight into how the model processes the input data at each stage.

For the ETTh1 in Figure 4, the input sequence length is 512, and we display the last 100 time steps of the input. The prediction length is set to 96. We select five samples from the ETTh1 dataset, and for each sample, we visualize the attention maps for stage 1 and stage 2 of the SSA. From the attention maps, it is evident that there are significant variations in the attention distributions across different samples. Additionally, the

Table 12: Full long-term forecasting results. We set the forecasting horizons $H \in \{96, 192, 336, 720\}$. A lower value indicates better performance. Avg means the average results from all prediction lengths. Red: the best, Blue lined: the second best.

Models		PSformer		SAMformer		TSMixer		PatchTST		MOMENT		ModernTCN		FEDformer		GPT4TS		Autoformer		RLinear		iTransformer	
Metric		MSE	MAE	MSE	MAE	MSE	MAE	MSE	MAE	MSE	MAE	MSE	MAE	MSE	MAE	MSE	MAE	MSE	MAE	MSE	MAE	MSE	MAE
ETTh1	96	0.352	0.385	0.381	0.402	0.388	0.408	0.414	0.419	0.387	0.410	0.373	0.399	0.376	0.415	0.376	0.397	0.435	0.446	0.386	0.395	0.386	0.405
	192	0.385	0.406	0.409	0.418	0.421	0.426	0.460	0.445	0.410	0.426	0.407	0.419	0.423	0.446	0.416	0.418	0.456	0.457	0.437	0.424	0.441	0.436
	336	0.411	0.424	0.423	0.425	0.430	0.434	0.501	0.466	0.422	0.437	0.436	0.437	0.444	0.462	0.442	0.433	0.486	0.487	0.479	0.446	0.487	0.458
	720	0.440	0.456	0.427	0.449	0.440	0.459	0.500	0.488	0.454	0.472	0.467	0.474	0.469	0.492	0.477	0.515	0.515	0.517	0.481	0.470	0.503	0.491
	Avg	0.397	0.418	0.410	0.424	0.420	0.431	0.468	0.455	0.418	0.436	0.421	0.432	0.428	0.454	0.428	0.426	0.473	0.477	0.446	0.434	0.454	0.448
ETTh2	96	0.272	0.337	0.295	0.358	0.305	0.367	0.302	0.348	0.288	0.345	0.271	0.339	0.332	0.374	0.285	0.342	0.332	0.368	0.288	0.338	0.297	0.349
	192	0.335	0.379	0.340	0.386	0.350	0.393	0.388	0.400	0.349	0.386	0.332	0.382	0.407	0.446	0.354	0.389	0.426	0.434	0.374	0.390	0.380	0.400
	336	0.356	0.411	0.350	0.395	0.360	0.404	0.426	0.433	0.369	0.408	0.365	0.411	0.400	0.447	0.373	0.407	0.477	0.479	0.415	0.426	0.428	0.432
	720	0.389	0.431	0.391	0.428	0.402	0.435	0.431	0.446	0.403	0.439	0.402	0.441	0.412	0.469	0.406	0.441	0.453	0.490	0.420	0.440	0.427	0.445
	Avg	0.338	0.390	0.344	0.391	0.354	0.400	0.387	0.407	0.352	0.394	0.343	0.393	0.388	0.434	0.355	0.395	0.422	0.443	0.374	0.398	0.383	0.407
ETTm1	96	0.282	0.336	0.329	0.363	0.327	0.363	0.329	0.367	0.293	0.349	0.310	0.356	0.326	0.390	0.292	0.346	0.510	0.492	0.355	0.376	0.334	0.368
	192	0.321	0.360	0.353	0.378	0.356	0.381	0.367	0.385	0.326	0.368	0.340	0.373	0.365	0.415	0.332	0.372	0.514	0.495	0.391	0.392	0.377	0.391
	336	0.352	0.380	0.382	0.394	0.387	0.397	0.399	0.410	0.352	0.384	0.373	0.392	0.392	0.425	0.366	0.394	0.510	0.492	0.424	0.415	0.426	0.420
	720	0.413	0.412	0.429	0.418	0.441	0.425	0.454	0.439	0.405	0.416	0.420	0.418	0.446	0.458	0.417	0.421	0.527	0.492	0.487	0.450	0.491	0.459
	Avg	0.342	0.372	0.373	0.388	0.378	0.392	0.387	0.400	0.344	0.379	0.361	0.384	0.382	0.422	0.351	0.383	0.515	0.493	0.414	0.407	0.407	0.410
ETTm2	96	0.167	0.258	0.181	0.274	0.190	0.284	0.175	0.259	0.170	0.260	0.168	0.261	0.180	0.271	0.173	0.262	0.205	0.293	0.182	0.265	0.180	0.264
	192	0.219	0.292	0.233	0.306	0.250	0.320	0.241	0.302	0.227	0.297	0.231	0.305	0.252	0.318	0.229	0.301	0.278	0.336	0.246	0.304	0.250	0.309
	336	0.269	0.325	0.285	0.338	0.301	0.350	0.305	0.343	0.275	0.328	0.272	0.328	0.324	0.364	0.286	0.341	0.343	0.379	0.307	0.342	0.311	0.348
	720	0.347	0.376	0.375	0.390	0.389	0.402	0.402	0.400	0.363	0.387	0.375	0.394	0.410	0.420	0.378	0.401	0.414	0.419	0.407	0.398	0.412	0.407
	Avg	0.251	0.313	0.269	0.327	0.283	0.339	0.281	0.326	0.259	0.318	0.262	0.322	0.292	0.343	0.267	0.326	0.310	0.357	0.286	0.327	0.288	0.332
Weather	96	0.149	0.200	0.197	0.249	0.189	0.242	0.177	0.218	0.154	0.209	0.154	0.209	0.238	0.314	0.162	0.212	0.249	0.329	0.192	0.232	0.174	0.214
	192	0.193	0.243	0.235	0.277	0.228	0.272	0.225	0.259	0.197	0.248	0.207	0.257	0.275	0.329	0.204	0.248	0.325	0.370	0.240	0.271	0.221	0.254
	336	0.245	0.282	0.276	0.304	0.271	0.299	0.278	0.297	0.246	0.285	0.248	0.289	0.339	0.377	0.254	0.286	0.351	0.391	0.292	0.307	0.278	0.296
	720	0.314	0.332	0.334	0.342	0.331	0.341	0.354	0.348	0.315	0.336	0.337	0.342	0.389	0.409	0.326	0.337	0.415	0.426	0.364	0.353	0.358	0.347
	Avg	0.225	0.264	0.261	0.293	0.255	0.289	0.259	0.281	0.228	0.270	0.237	0.274	0.310	0.357	0.237	0.271	0.335	0.379	0.272	0.291	0.258	0.278
Electricity	96	0.133	0.229	0.155	0.252	0.171	0.273	0.181	0.270	0.136	0.233	0.133	0.228	0.186	0.302	0.139	0.238	0.196	0.313	0.201	0.281	0.148	0.240
	192	0.149	0.242	0.168	0.263	0.191	0.292	0.188	0.274	0.152	0.247	0.147	0.241	0.197	0.311	0.153	0.251	0.211	0.324	0.201	0.283	0.162	0.253
	336	0.164	0.258	0.183	0.277	0.198	0.297	0.204	0.293	0.167	0.264	0.163	0.260	0.213	0.328	0.169	0.266	0.214	0.327	0.215	0.298	0.178	0.269
	720	0.203	0.291	0.219	0.306	0.230	0.321	0.246	0.324	0.205	0.295	0.194	0.289	0.233	0.344	0.206	0.297	0.236	0.342	0.257	0.331	0.225	0.317
	Avg	0.162	0.255	0.181	0.275	0.198	0.296	0.205	0.290	0.165	0.260	0.160	0.255	0.207	0.321	0.167	0.263	0.214	0.327	0.219	0.298	0.178	0.270
Exchange	96	0.081	0.197	0.161	0.306	0.233	0.363	0.088	0.205	0.098	0.224	0.207	0.342	0.139	0.276	0.091	0.212	0.197	0.323	0.093	0.217	0.086	0.206
	192	0.179	0.299	0.246	0.371	0.342	0.437	0.176	0.299	0.201	0.323	0.337	0.437	0.256	0.369	0.183	0.304	0.300	0.369	0.184	0.307	0.177	0.299
	336	0.328	0.412	0.368	0.453	0.474	0.515	0.301	0.397	0.387	0.454	0.520	0.553	0.426	0.464	0.328	0.417	0.509	0.524	0.351	0.432	0.331	0.417
	720	0.842	0.689	1.003	0.750	1.078	0.777	0.901	0.714	1.062	0.783	1.154	0.810	1.090	0.800	0.880	0.704	1.447	0.941	0.886	0.714	0.847	0.691
	Avg	0.358	0.399	0.445	0.470	0.532	0.523	0.367	0.404	0.437	0.446	0.555	0.536	0.478	0.477	0.371	0.409	0.613	0.539	0.378	0.417	0.360	0.403
Traffic	96	0.367	0.257	0.407	0.292	0.409	0.300	0.462	0.295	0.391	0.282	0.391	0.271	0.576	0.359	0.388	0.282	0.597	0.371	0.649	0.389	0.395	0.268
	192	0.390	0.272	0.415	0.294	0.433	0.317	0.466	0.296	0.404	0.287	0.403	0.275	0.610	0.380	0.407	0.290	0.607	0.382	0.601	0.366	0.417	0.276
	336	0.404	0.274	0.421	0.292	0.424	0.299	0.482	0.304	0.414	0.292	0.410	0.280	0.608	0.375	0.412	0.294	0.623	0.387	0.609	0.369	0.433	0.283
	720	0.439	0.294	0.456	0.311	0.488	0.344	0.514	0.322	0.450	0.310	0.451	0.305	0.621	0.375	0.450	0.312	0.639	0.395	0.647	0.387	0.467	0.302
	Avg	0.400	0.274	0.425	0.297	0.439	0.315	0.481	0.304	0.415	0.293	0.414	0.283	0.604	0.372	0.414	0.295	0.617	0.384	0.626	0.378	0.428	0.282
1st Count		20	22	2	3	0	0	2	3	2	0	6	3	0	0	0	0	0	0	0	0	2	2

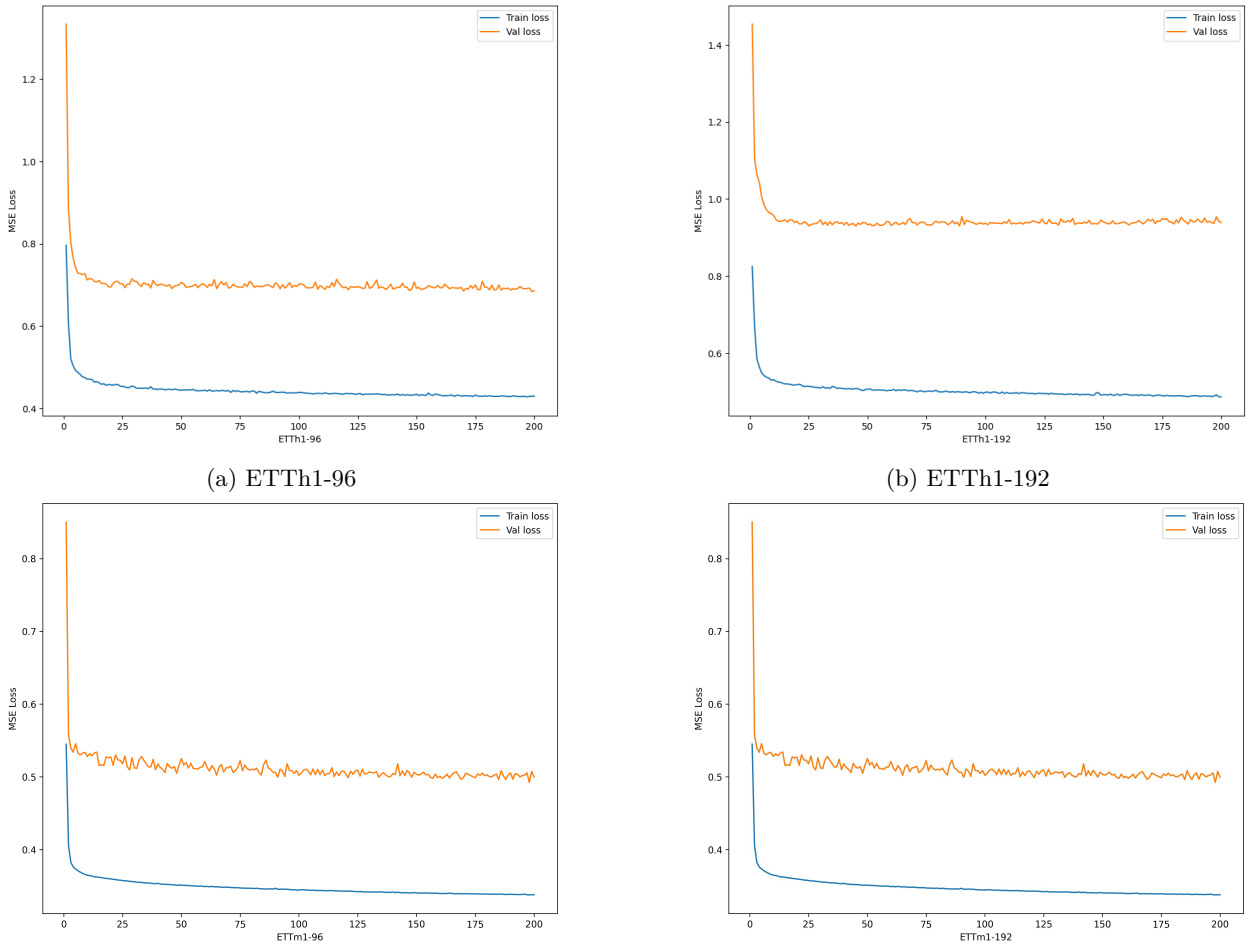

(a) ETTh1-96

(b) ETTh1-192

(c) ETTm1-96

(d) ETTm1-192

Figure 3: Training and validation loss curves of the ETTh1 and ETTm1 datasets.

attention maps from stage 1 and stage 2 also show noticeable differences, despite both stages sharing the same PS block parameters. This indicates that while the two-stage share parameters, they are able to handle and process the information differently, capturing different aspects of the input data at each stage of the model.

For the Weather in Figure 5, the input length is also 512, and the last 100 time steps are displayed, while the prediction length is 192. Since the model for this dataset employs a three-layer Encoder structure, we display the attention maps for both stages across each layer. Specifically, the notation“1-2" represents the attention map for layer 1, stage 2, and similarly for the other layers. The first two rows of attention maps correspond to the attention distributions from the three Encoder layers. Following that, the prediction curves for nine selected variates are plotted, providing a detailed view of the model's forecast performance across different variates.

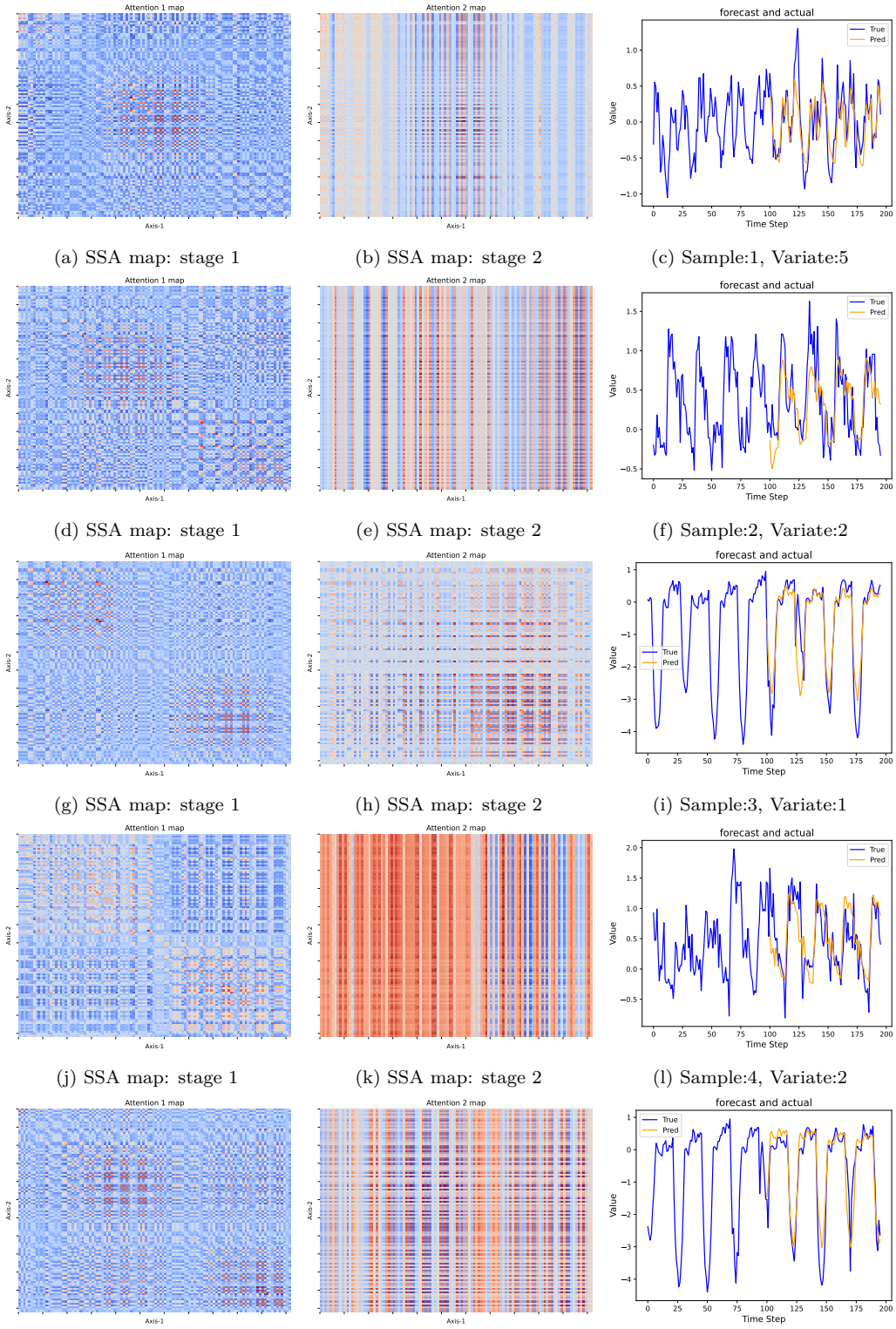

(a) SSA map: stage 1 (b) SSA map: stage 2 (c) Sample:1, Variate:5

(d) SSA map: stage 1 (e) SSA map: stage 2 (f) Sample:2, Variate:2

(g) SSA map: stage 1 (h) SSA map: stage 2 (i) Sample:3, Variate:1

(j) SSA map: stage 1 (k) SSA map: stage 2 (l) Sample:4, Variate:2

(m) SSA map: stage 1 (n) SSA map: stage 2 (o) Sample:5, Variate:1

Figure 4: SSA map and forecast samples for ETTh1-96

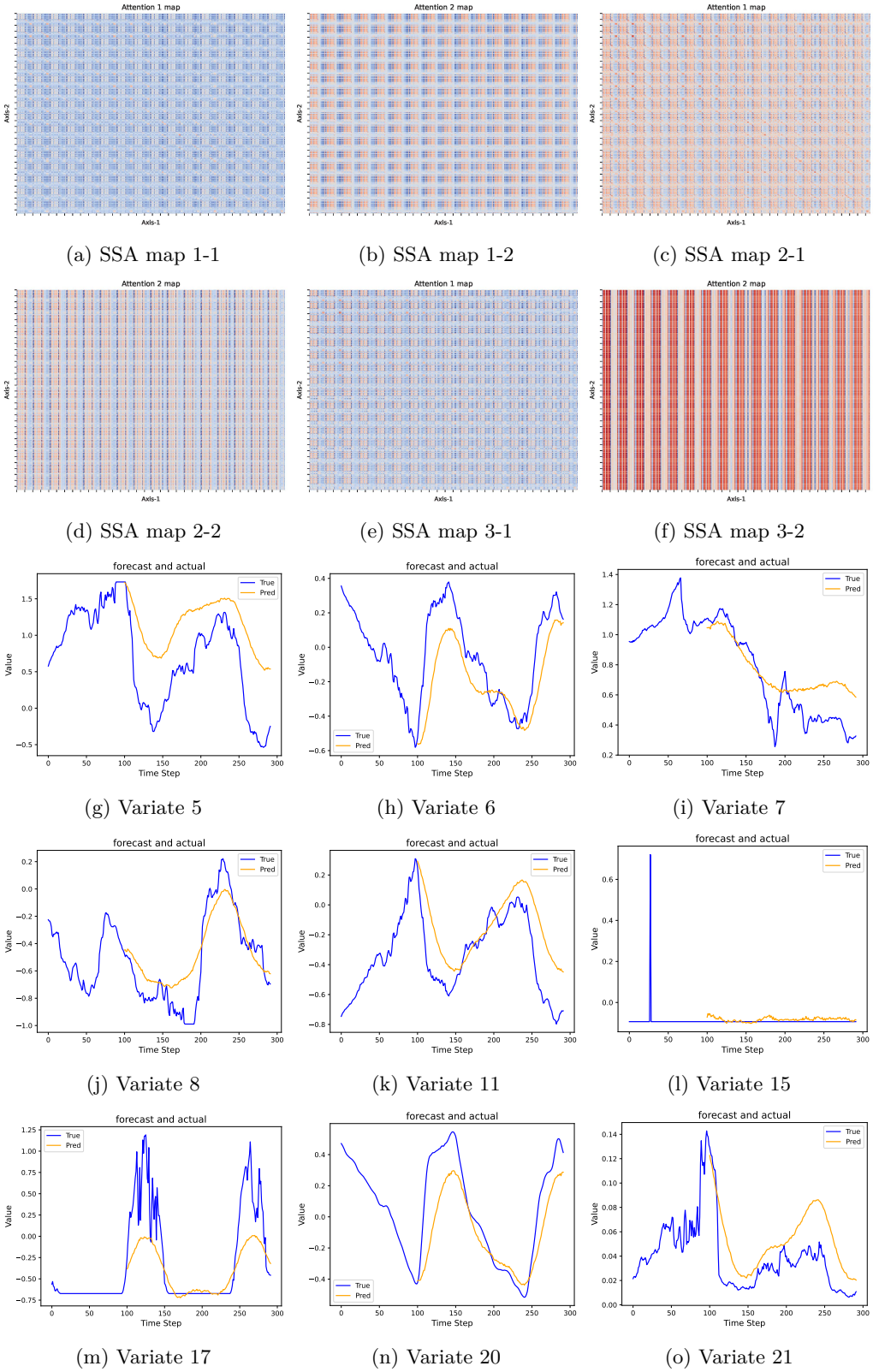

(a) SSA map 1-1 (b) SSA map 1-2 (c) SSA map 2-1

(d) SSA map 2-2 (e) SSA map 3-1 (f) SSA map 3-2

(g) Variate 5 (h) Variate 6 (i) Variate 7

(j) Variate 8 (k) Variate 11 (l) Variate 15

(m) Variate 17 (n) Variate 20 (o) Variate 21

Figure 5: SSA matrices and forecast for Weather-192

B.5 Additional Visualization of Attention Map

We further analyze the SSA attention matrix of PSformer in both the temporal and spatial dimensions. Using samples from ETTh1, the key parameters include: input length $L = 512$, segment number $N = 32$, channel number $M = 7$, and patch length $P = 16$. Therefore, $QK^T \in R^{C \times C}$, where $C = M \times P$, as described in the Spatial-Temporal Segment Attention part.

B.5.1 Additional Visualization of the SSA Attention

Since stage one of SSA operates on the input data x, we print out the attention matrix to observe how SSA captures local spatio-temporal information. The attention matrix is shown in the Figure 8 below. To better display the colors, we choose the plasma color style and apply a clipping operation to the top 1.

Since both the x-axis and y-axis correspond to a specific point within a segment of length C, the brighter yellow points in this attention matrix indicate higher attention weights between the corresponding x-axis and y-axis positions. Taking this attention map as an example, we can observe distinct high-attention regions (e.g., the top-left corner) and high-attention areas between different time steps and variables (e.g., the non-diagonal symmetric grid section in the top-left corner). From this, we can observe that the coordinate positions within the spatial attention submatrix (inside the grids) exhibit the same or gradually changing attention weights across different time steps (between the grids). This suggests that the model may capture temporal consistency between variables, local stationary features, and long-term dependencies across time steps.

B.5.2 Single-channel Attention Map

For better visualization of SSA's capture of the local temporal dimension, we extract the single-channel attention submatrix from the attention matrix, as shown in the upper corner of the Figure 7, and visualize the corresponding single-channel local time sequence in the lower corner of the Figure 7. This allows us to observe the high-attention weights at specific temporal local positions. We present three samples of attention along the temporal dimension for a single sequence.

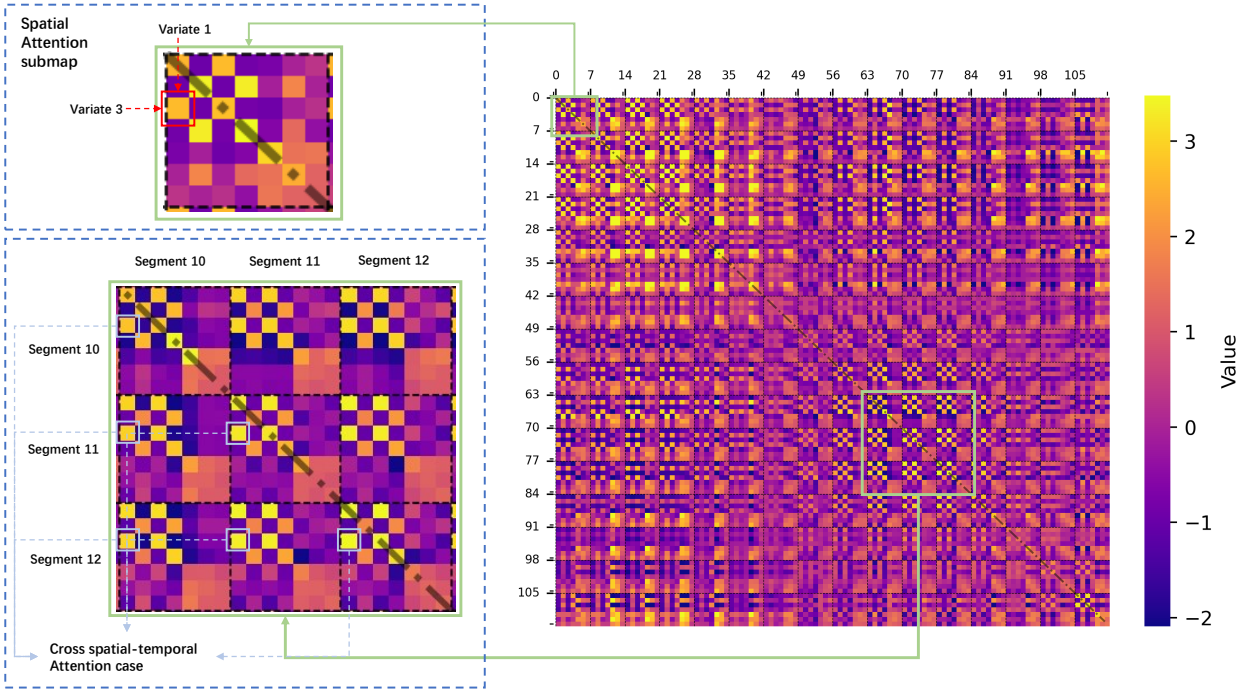

Figure 6: SSA attention map.

From the upper-left corner of Figure 7, the high attention weight at coordinates (x=7, y=14) corresponds to time steps 7 and 14 in the lower-left corner of Figure 7. These two time points represent a pattern of significant change in the sequence, which the model identifies as a high attention weight.

Using the same analysis method, we can observe in the middle column of the Figure 7 that high attention occurs between time steps 2 and 3, as well as between time steps 9 and 10. This includes both consecutive time points with related attention (e.g., 2 and 3) and attention with intervals (e.g., 2-3 and 9-10), which correspond to the upward phase and the stable phase of the time series.

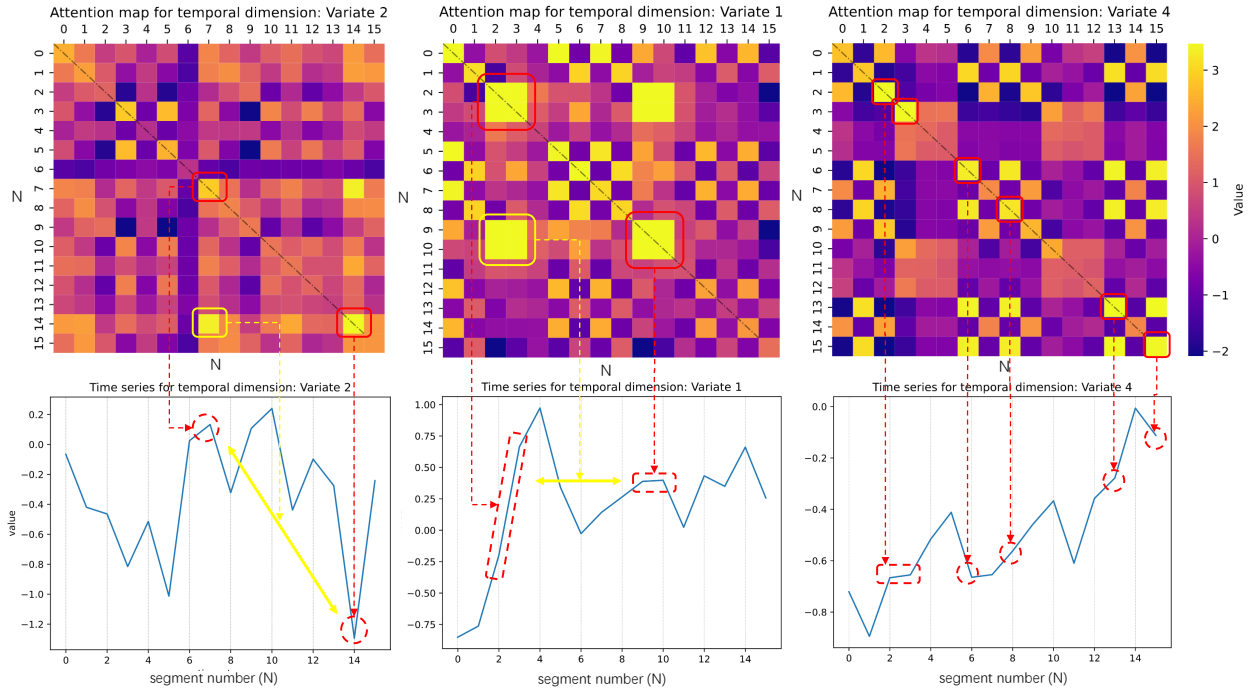

Figure 7: SSA intra-channel attention submap.

B.5.3 Cross-channels Attention Map

To visualize the cross-channel attention relationships in SSA, we extract the attention weights between two channels, forming the corresponding cross-channel attention submatrix map and the time series plots for the two variables, as shown in Figure 8.

From upper-left of the Figure 8, we can see that high attention is mainly concentrated at coordinates (3, 14) and (5, 14), which correspond to time step 14 of variate 2 and time steps 3 and 5 of variate 0. These three positions may reflect local minima for the two time series. In the middle column, the high attention weights correspond to large changes in opposite directions between variate 0 and variate 6. In the right column of Figure 8, we can see that the segments corresponding to segment numbers 1 and 2 of variate 5 exhibit higher attention values compared to the overall variate 0. Additionally, the attention on time steps 4 and 5, as well as 11 and 12, of variate 0 is higher.

B.5.4 Additional Visualization of the SSA Attention Map without Parameter Sharing

We further analyzed how parameter sharing affects the model's ability to capture temporal patterns by comparing attention maps with and without parameter sharing. To achieve this, we also visualized the attention heatmaps without parameter sharing. To reflect cross-layer variations, we provided attention maps from both the first and second layers for comparison, as in Figure 9a and Figure 9b. Several differences were observed when comparing these to the attention maps with parameter sharing.

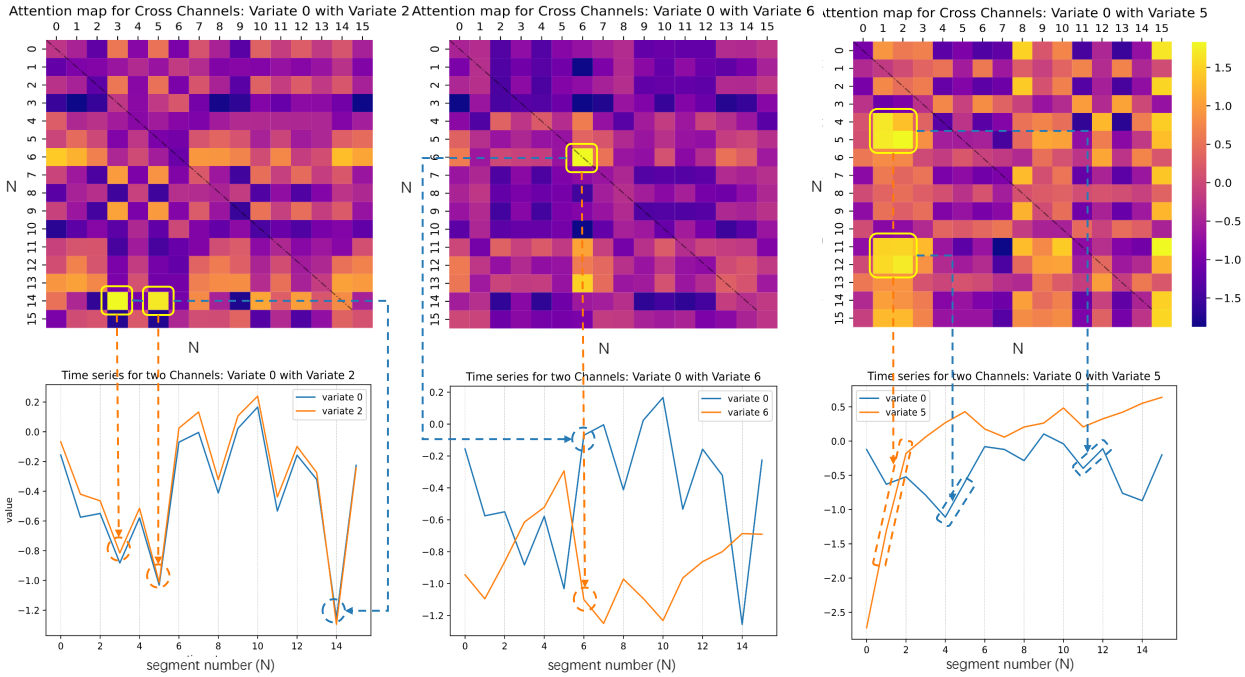

Figure 8: SSA cross-channel attention submap.

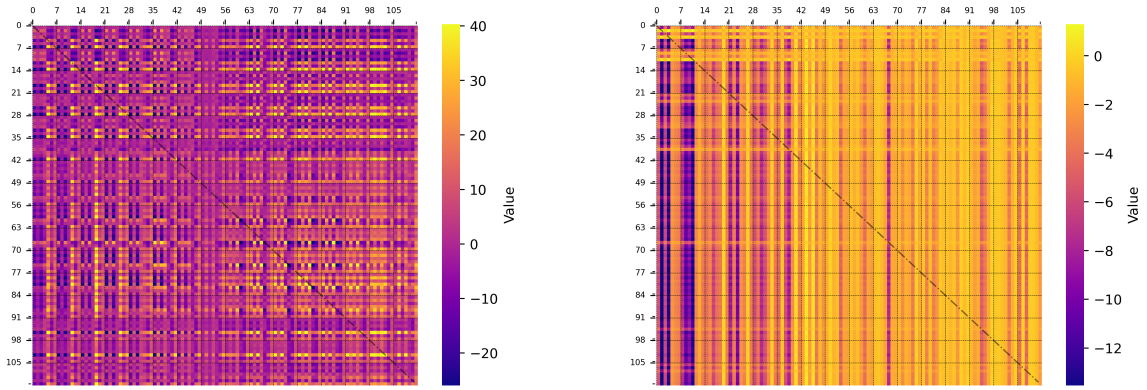

(a) Attention1 map without parameter sharing.

(b) Attention2 map without parameter sharing.

Figure 9: Comparison of Variate 2 Attention Maps

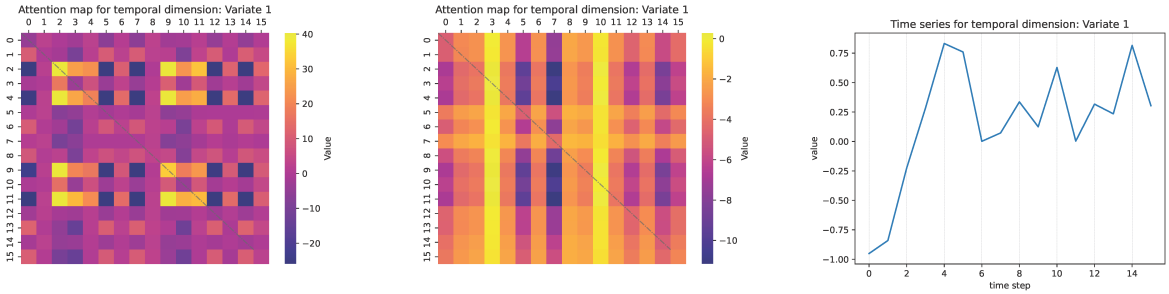

(a) Attention1 map for Variate 2. (b) Attention2 map for Variate 2. (c) Time series for Variate 2.

Figure 10: Single-channel Attention Map without Parameter Sharing.

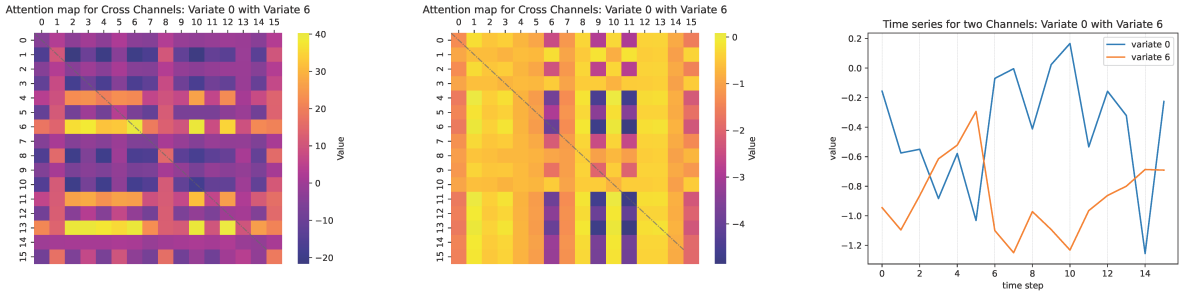

(a) Attention1 map for Variate 2. (b) Attention2 map for Variate 2. (c) Time series for Variate 2.

Figure 11: Comparison of Cross-channels Attention Maps without Parameter Sharing.

Range of attention weights: For attention maps with parameter sharing, the values generally range between [-3, 3], while for those without parameter sharing, the range is much broader, approximately [-30, 40]. The larger variations in attention weights without parameter sharing might contribute to faster model convergence during training.

Inter-channel relationships: With parameter sharing, the inter-channel relationships represented in Figure 10 are simpler and more distinct. Gradual transitions in attention weights between grid cells are clearly visible. In contrast, without parameter sharing, although progressive changes are still observed, the temporal relationships become more complex and harder to interpret (as the attention map in the first layer cannot be directly aligned with the corresponding temporal positions due to the lack of parameter sharing).

Cross-layer variations: Observing the differences between the two layers in the non-parameter-shared attention maps in Figure 11, I tend to suggest that the first layer's attention focuses on capturing basic temporal patterns, which are then refined and processed in the second layer. However, the interpretability in temporal models is challenging and remains an open research question worthy of further exploration.

B.6 SSA for univariate time series and low dependency series

We tested the performance of PSformer in single-sequence forecasting. Specifically, we saved the 8 variables from the Exchange dataset into 8 separate single-sequence files, each supplemented with an additional column filled with zeros to form single sequences, along with an unrelated variable. We compared PSformer with the baseline model PatchTST (which is channel-independent and performs well on the Exchange dataset).

The experimental results in the Table 13. As can be observed, PSformer consistently outperforms across all uni-variate time series, demonstrating that the PSformer architecture is not only effective in capturing cross-channel information but also performs well in univariate time series or with little dependency between variables.

Table 13: Performance comparison between PSformer and PatchTST across various variates.

Variate	Model	96	192	336	720
1	PSformer	0.057	0.147	0.360	0.803
	PatchTST	0.063	0.152	0.461	-
2	PSformer	0.042	0.094	0.152	0.216
	PatchTST	0.052	0.140	0.181	-
3	PSformer	0.034	0.093	0.169	0.476
	PatchTST	0.055	0.116	0.176	-
4	PSformer	0.041	0.066	0.090	0.146
	PatchTST	0.058	0.085	0.111	-
5	PSformer	0.007	0.009	0.012	0.073
	PatchTST	0.016	0.025	0.022	-
6	PSformer	0.077	0.169	0.532	1.125
	PatchTST	0.099	0.215	0.505	-
7	PSformer	0.033	0.069	0.120	0.342
	PatchTST	0.039	0.079	0.140	-
OT	PSformer	0.047	0.101	0.190	0.510
	PatchTST	0.097	0.154	0.230	-

Table 14: Performance comparison with different norm window sizes on the Exchange Rate dataset.

Dataset	Horizon	16	64	128	256	512
Exchange Rate	96	0.081	0.085	0.090	0.092	0.091
	192	0.179	0.187	0.189	0.191	0.197
	336	0.328	0.338	0.356	0.362	0.345
	720	0.842	0.900	0.976	1.003	1.036
	Avg	0.358	0.378	0.403	0.412	0.417

During the experiments, PatchTST encountered a NaN loss on the validation set for a prediction length of 720, so the corresponding loss value was not recorded.

B.7 Exchange datesets performance with different RevIN look-back windows

The Exchange dataset is non-stationary nature and random walk characteristics, which prevent RevIN from obtaining stable mean and variance statistics. These statistics are sensitive to the choice of RevIN's lookback window. Further testing in the Table 14 revealed that the model performs best when the lookback window for calculating RevIN's statistics is very small (length 16), achieving results superior to all selected baseline models. We believe that for non-stationary data, RevIN's normalization should be used with caution. Adjusting the lookback window length can help identify more stable statistical means and variances, thereby facilitating model training.

B.8 Comparasion with Additional Baselines (Part-I).

B.8.1 Comparison with Extended Baselines

We have collected the Extended experimental MSE loss results of the relevant models in Table 15. Although there are differences in experimental setups across each work, which may affect the results and prevent a completely fair comparison, we have provided some key settings to help better understand the model performance.

From the results, compared to models with fixed windows, PSformer performed best on 7/8 of the prediction tasks. This further highlights PSformer's competitive performance in forecasting. Even when compared to non-fixed window models like FITS, PSformer performed best on 4/7 of the prediction tasks.

B.8.2 Comparison with Additional Baselines (Part-II)

We have collected the Extended experimental results of the relevant models in Table 16. Comparison with PDF and PatchTST. We set PDF and PatchTST with same setting (input length to 512, $drop_last = False$). The results provide further insights into PSformer performance.

We conducted tests on the following five datasets. From the experimental results, both PSformer and PDF significantly outperform PatchTST in predictive performance, and PSformer achieving better predictions than PDF. However, the average prediction loss reduction relative to PDF is not substantial. Therefore, we consider PSformer and PDF to exhibit equally excellent predictive performance under the same settings.

Comparison with Time-LLM. For Time-LLM, We listed the predictive performance from the original paper of the model in the table below. However, we check its offical repository and find Time-LLM also faces DL issue in the test set dataloader, which may affects its reported results. Besides, due to the computational demands of large-scale models, we decided not to execute its code directly in our experiments. When selecting the baseline large models, we considered both MOMENT and TimeLLM. We ultimately chose MOMENT for two main reasons: the MOMENT paper includes a direct comparison with TimeLLM, and it is relatively lightweight (428M parameters). In summary, despite the significant difference in parameter scale and the DL issue present in TimeLLM, PSformer still achieves equal or better average predictive performance than TimeLLM on 3 out of 5 datasets.

B.9 Comparisons of convergence rates with and without parameter sharing.

We compare the impact of parameter sharing on the convergence rate using the ETTh1 and Exchange datasets, recording the total number of epochs and the MSE loss under the same settings.

The experimental results are shown in the Table 17, where the values represent epochs/MSE loss. We observe that the number of epochs required with or without parameter sharing on the ETTh1 dataset varies depending on the prediction length. However, for the Exchange dataset, the convergence rate is faster without parameter sharing.

Additionally, in terms of MSE loss, using parameter sharing leads to greater reductions in loss and also results in fewer parameters. Therefore, there exists a trade-off between convergence rates, loss reduction, and parameter efficiency.

B.10 Testing of Parameter-Saving Capacity for Pre-Trained Models

For further validating the framework's parameter-saving capacity, we compared the parameter count of the PSformer under Parameter Sharing and No Parameter Sharing scenarios, including the comparison for 1-layer and 3-layer Encoders, as well as for different layers same as GPT2 models (GPT2-small, GPT2-medium, GPT2-large, and GPT2-xl) at 12-layer, 24-layer, 36-layer, and 48-layer configurations. The results are reported in the Table 18. In addition, if the hidden layer dimension is expanded from 32 to 1024 (as in GPT2), or if multi-head attention is adopted, the total number of parameters will also increase significantly.

Table 15: Comparasion with additional baselines (Part-I).

	Models	**PSformer**	**TimeMixer**	**CrossGNN**	**MICN**	**TimesNet**	**FITS**
ETTh1	**96**	0.352	0.375	0.382	\	0.384	0.372
	192	0.385	0.429	0.427	\	0.436	0.404
	336	0.411	0.484	0.465	\	0.491	0.427
	720	0.44	0.498	0.472	\	0.521	0.424
	Avg	0.397	0.447	0.437	\	0.458	0.407
ETTh2	**96**	0.272	0.289	0.309	\	0.34	0.271
	192	0.335	0.372	0.39	\	0.402	0.331
	336	0.356	0.386	0.426	\	0.452	0.354
	720	0.389	0.412	0.445	\	0.462	0.377
	Avg	0.338	0.365	0.393	\	0.414	0.333
ETTm1	**96**	0.282	0.32	0.335	\	0.338	0.303
	192	0.321	0.361	0.372	\	0.372	0.337
	336	0.352	0.39	0.403	\	0.41	0.366
	720	0.413	0.454	0.461	\	0.478	0.415
	Avg	0.342	0.381	0.393	\	0.4	0.355
ETTm2	**96**	0.167	0.175	0.176	0.179	0.187	0.162
	192	0.219	0.237	0.24	0.307	0.249	0.216
	336	0.269	0.298	0.304	0.325	0.321	0.268
	720	0.347	0.391	0.406	0.502	0.408	0.348
	Avg	0.251	0.275	0.282	0.328	0.291	0.249
Weather	**96**	0.149	0.163	0.159	\	0.172	0.143
	192	0.193	0.208	0.211	\	0.219	0.186
	336	0.245	0.251	0.267	\	0.28	0.236
	720	0.314	0.339	0.352	\	0.365	0.307
	Avg	0.225	0.24	0.247	\	0.259	0.218
Electricity	**96**	0.133	0.153	0.173	0.164	0.168	0.134
	192	0.149	0.166	0.195	0.177	0.184	0.149
	336	0.164	0.185	0.206	0.193	0.198	0.165
	720	0.203	0.225	0.231	0.212	0.22	0.203
	Avg	0.162	0.182	0.201	0.187	0.192	0.163
Exchange rate	**96**	0.091	0.09	0.084	0.102	0.107	\
	192	0.197	0.187	0.171	0.172	0.226	\
	336	0.345	0.353	0.319	0.272	0.367	\
	720	1.036	0.934	0.805	0.714	0.964	\
	Avg	0.417	0.391	0.345	0.315	0.416	\
Traffic	**96**	0.367	0.462	0.57	0.519	0.593	0.385
	192	0.39	0.473	0.577	0.537	0.617	0.397
	336	0.404	0.498	0.588	0.534	0.629	0.41
	720	0.439	0.506	0.597	0.577	0.64	0.448
	Avg	0.4	0.485	0.583	0.542	0.62	0.41

Table 16: Comparison with additional baselines (Part-II).

	Models	**PSformer**	**Crossformer**	**PDF**	**PatchTST**	**TimeLLM**
ETTh1	**96**	0.352	0.384	0.361	0.374	0.362
	192	0.385	0.438	0.391	0.413	0.398
	336	0.411	0.495	0.415	0.434	0.43
	720	0.44	0.522	0.468	0.455	0.442
	Avg	0.397	0.46	0.409	0.419	0.408
ETTh2	**96**	0.272	0.347	0.272	0.274	0.268
	192	0.335	0.419	0.334	0.341	0.329
	336	0.356	0.449	0.357	0.364	0.368
	720	0.389	0.479	0.397	0.39	0.372
	Avg	0.338	0.424	0.34	0.342	0.334
ETTm1	**96**	0.282	0.349	0.284	0.29	0.272
	192	0.321	0.405	0.327	0.333	0.31
	336	0.352	0.432	0.351	0.37	0.352
	720	0.413	0.487	0.409	0.416	0.383
	Avg	0.342	0.418	0.343	0.352	0.329
ETTm2	**96**	0.167	0.208	0.162	0.166	0.161
	192	0.219	0.263	0.224	0.223	0.219
	336	0.269	0.337	0.277	0.273	0.271
	720	0.347	0.429	0.354	0.363	0.352
	Avg	0.251	0.309	0.254	0.256	0.251
Weather	**96**	0.149	0.191	0.147	0.152	0.147
	192	0.193	0.219	0.191	0.196	0.189
	336	0.245	0.287	0.243	0.247	0.262
	720	0.314	0.368	0.317	0.315	0.304
	Avg	0.225	0.266	0.225	0.228	0.226

Table 17: Comparisons of convergence rates.

	methods	96	192	336	720
ETTh1	w parameter sharing	83/0.352	70/0.385	53/0.411	35/0.440
	w/o parameter sharing	46/0.359	108/0.392	39/0.423	36/0.441
Exchange	w parameter sharing	71/0.081	51/0.179	82/0.328	32/0.842
	w/o parameter sharing	47/0.084	32/0.183	43/0.333	31/0.855

Table 18: Comparisons of Parameter-Saving Capacity.

	1	3	12	24	36	48
Parameter Sharing	52,416	58,752	87,264	125,280	163,296	201,312
No Parameter Sharing	71,424	115,776	315,360	581,472	847,584	1,113,696

B.11 Discuss about parameter search space.

The main hyperparameters of PSformer include: 1. the number of encoders, 2. the number of segments, and 3. the SAM hyperparameter rho. For the number of encoders, we primarily searched within 1 to 3 layers. For the number of segments, we maintain the same as the number of patches in PatchTST, we also analyzed values that divide the input length evenly (specifically: 2, 4, 8, 16, 32, 64, 128, 256), and ultimately set all prediction tasks to 32 to avoid performance improvements caused by complex hyperparameter tuning. For the SAM hyperparameter rho, we referred to SAMformer and performed a search across 11 parameter points evenly spaced in the range 0 to 1. The number of encoders and segments can be found in the ablation study in section 4.2. Additionally, for the learning rate, we mainly tested values of $1e-3$ and $1e-4$, and for the learning rate scheduler, we tested OneCycle and MultiStepLR.